Chapter in **Advancing Astrophysics with the SKA – II**

Radio Galaxies and Jet Duty Cycles

M. J. Hardcastle[1], C. Konar[2], S. Dutta[3], D. V. Lal[4], R. D. Baldi[5], M. Brienza[5], A. Hota[6], M. Kunert-Bajraszewska[7], B. Mingo[1], M. Pandey-Pommier[8], K. Rubinur[9], S. Shabala[10] and E. Vardoulaki[11]

[1]*Centre for Astrophysics Research, Department of Physics, Astronomy and Mathematics, University of Hertfordshire, College Lane, Hatfield AL10 9AB, UK*

[2]*Department of Physics, Amity Institute of Applied Sciences, Amity University Uttar Pradesh, Sector-125, Noida 201313, U.P., India*

[3]*The Inter-University Institute for Data Intensive Astronomy (IDIA), and University of Cape Town, Private Bag X3, Rondebosch, Cape Town 7701, South Africa*

[4]*National Centre for Radio Astrophysics - Tata Institute of Fundamental Research Post Box 3, Ganeshkhind P.O., Pune 411007, India*

[5]*INAF - Istituto di Radioastronomia, Via P. Gobetti 101, I-40129, Bologna, Italy*

[6]*UM-DAE Centre for Excellence in Basic Sciences, University of Mumbai, Santacruz-East, Mumbai 400098, India*

[7]*Institute of Astronomy, Faculty of Physics, Astronomy and Informatics, NCU, Grudziądzka 5/7, 87-100, Toruń, Poland*

[8]*Scientific Centre, Catholic University of Lyon, 10 Place des Archives 69288, Lyon, France*

[9]*Institute of Theoretical Astrophysics, University of Oslo, Postboks 1029, Blindern, 0315 Oslo, Norway*

[10]*School of Natural Sciences, University of Tasmania, Private Bag 37, Hobart 7001, Australia*

[11]*National Observatory Athens, Hill of the Nymphs, Athens, Greece*

E-mail: m.j.hardcastle@herts.ac.uk, chiranjib.konar@gmail.com, sushant.dutta@uct.ac.za, dharam@ncra.tifr.res.in, ranieri.baldi@inaf.it, marisa.brienza@inaf.it, hotaananda@gmail.com, magda@astro.umk.pl, b.mingo@herts.ac.uk, mamtapommier@gmail.com, rubinur.khatun@astro.uio.no, stanislav.shabala@utas.edu.au, elenivard@gmail.com

Radio-luminous active galactic nuclei, or radio galaxies, are the brightest population of objects in the extragalactic radio sky and will be seen in large numbers in essentially every SKA observation. Despite having been studied for more than seventy years, some aspects of radio galaxy physics are still poorly understood, and the SKA will shed light on this by enabling the generation of very large samples of high-resolution, sensitive, broad-band images of radio galaxies, allowing us to probe, for example, regions of particle acceleration, spectral ageing, and the magnetic field structures both internal and external to the radio lobes. A key feature of the radio galaxy population is that observations of extended sources probe the past history, and thus the duty cycles, of accretion onto the central supermassive black hole, and we discuss ways in which the SKA will improve our understanding of episodic and dying radio galaxies in particular.

1 Introduction

Radio galaxies and radio-loud quasars, sometimes called radio-luminous active galactic nuclei (RLAGN) but referred to in this chapter simply as radio galaxies, are a type of active galactic nucleus (AGN) characterised by the fact that some or all of the nuclear activity emerges in the form of a high-speed collimated jet of energetic particles and magnetic fields. The synchrotron radio emission generated by these jets makes the galaxies hosting such AGN particularly luminous in the radio, giving them their name, but in fact emission from the jets and the large-scale structures they generate can be seen across the electromagnetic spectrum (e.g. Burbidge, 1956). Radio galaxies make up almost all of the brightest sources seen in extragalactic surveys, with the transition from radio galaxies to normal galaxies like the Milky Way (where radio emission is driven primarily by star-formation activity) occurring at the mJy level (Condon et al., 2002). Given the SKA's design, radio galaxies will be the brightest population of discrete sources in almost every continuum and polarization observation, whether they are the intended targets or not.

The study of radio galaxies is distinct from that of other types of active galaxies in several important ways. Firstly, the radio galaxy population offers our only view of the distant AGN population below the critical accretion rate (a few per cent of Eddington) at which accretion ceases to be radiatively efficient (Hardcastle et al., 2007; Best and Heckman, 2012; Mingo et al., 2014; Hardcastle, 2018a). While some radio AGN have all the apparatus of a radiatively efficient AGN, with a big blue bump, infrared-emitting torus, and X-ray corona, these radiatively efficient objects, known as radio-loud quasars or high-excitation radio galaxies (HERGs) and generally thought to accrete through a standard thin disk (Shakura and Sunyaev, 1973), are in the minority in the radio galaxy population. Much more common are the radiatively inefficient, low-excitation objects (LERGs) which are thought to accrete via an advection-dominated flow (e.g. Narayan and Yi, 1995). The low fraction of radiatively efficient objects is not surprising, since at any given time, far more of the supermassive black holes at the centres of galaxies are likely to be accreting at low rates than at high ones: the radio galaxy population gives almost the only way of studying this mode of accretion, sometimes referred to as low-luminosity AGN (LLAGN). However, going from radio observations to inferred accretion rates and thereby constraining the growth of these low-accretion rate black holes remains challenging. Jet generation almost certainly involves quantities such as the spin of the parent black hole and the magnetization of the accreting material (Blandford and Znajek, 1977) which are not directly constrained in most cases by observation at any waveband.

Secondly, radio galaxies can grow to large sizes (up to several Mpc: e.g. Mostert et al. 2024) in the course of their sometimes very long (up to $\sim$ 1 Gyr) active lifetimes, and their expansion through the interstellar and intergalactic media and potentially into intergalactic voids (Oei et al., 2024) allows the transport of energy, cosmic rays and magnetic fields from scales of the central black hole out to these very large distances. Particularly of interest to the galaxy formation and evolution community is their ability to heat the intracluster medium and so, through a feedback loop, prevent the cooling of hot gas and the subsequent formation of stars, thus playing a role in the truncation of the galaxy mass function at the high-mass end (e.g. Fabian, 2012; McNamara and Nulsen, 2012; Hardcastle and Croston, 2020; Magliocchetti, 2022; Eckert et al., 2024).

Thirdly, and this is the most important point for the remainder of the present chapter, radio galaxies

give us a unique view of the *history* of jet (and therefore, presumably, accretion) activity over the course of their lifetimes. Because the lobes of radio galaxies grow with time, it has long been realised (e.g. Baldwin, 1982) that they evolve along tracks in the power-linear size plot (the so-called *PD* diagram) which is in some sense analoguous to the Hertzsprung-Russell diagram for stars, and that these tracks can be predicted given some model of the evolution of the jets and their environment, for constant jet power (e.g. Kaiser et al. 1997; see Turner and Shabala (2023) for a review). It follows that distributions of source physical sizes can be used, with a model, to infer information about the distribution of active lifetimes of the population (e.g. Hardcastle et al., 2019b). In addition, observations of radio galaxies with evidence for multiple epochs of activity, so-called double-double radio galaxies (i.e. radio galaxies with a double pair of lobes with a single core, see Section 3 for details) or episodic radio galaxies (Schoenmakers et al., 2000) have given one of the few available pieces of information on the duty cycle of AGN activity: these objects show, in particular, that it is possible for the jet output to be initially high, drop to a low level, and then return to something like the original level on timescales that are short compared to the overall radio galaxy lifetime, presumably as a result of changes in accretion rate. In principle we can also detect the signatures of slower variations in jet power, for example a slow decrease over a source's lifetime, by looking for discrepancies betweeen the properties of the current energy dissipation regions (jets and hotspots) and the integrated properties of the lobes. In addition, the detection and characterization of remnant radio galaxies, where jet activity has completely ceased, is of great interest both because the evolution of these objects is very sensitive to the physics of synchrotron loss and expansion (Godfrey et al., 2017; Hardcastle, 2018b; Turner and Shabala, 2020b), and thus gives an important probe of the overall AGN duty cycle (Brienza et al., 2017; Shabala et al., 2020), and because the formation of a remnant is likely the precursor to mixing of the lobe cosmic rays through the intergalactic medium (Brienza et al., 2021; Lal, 2021). Finally, observations of resolved radio source morphology can give insights into the history of jet direction and therefore (presumably) black hole spin orientation, tracing both rapid changes in the jet axis due to black hole/black hole merger (Merritt and Ekers, 2002) and slow reorientation due to precession (e.g. Krause et al., 2019; Horton et al., 2020; Sebastian et al., 2024). A key question generally is how we can extract this information about accretion and jet orientation history from the radio observations.

In this chapter we will review the advances that will be made in understanding radio galaxy physics and life cycles using the completed phase 1 SKA (AA4), focusing particularly on the population of AGN that will be *resolved* with the SKA. We explore how we can (i) investigate the physical mechanisms driving jet production, (ii) constrain theoretical models that aim to explain the diversity of radio morphologies, (iii) find observational evidence for episodic jet activity, and (iv) constrain ages of radio-plasma by spectral ageing modelling to infer the duty cycle of episodic radio galaxies. We assess the feasibility of addressing the key questions by presenting our calculations of the sensitivity and resolution required throughout the chapter. We draw attention to other chapters in this volume that cover aspects of radio AGN science, in particular the chapters by Baczko et al. (2026), Baldi et al. (2026) and Panessa et al. (2026) which include discussion of radio AGN VLBI with the SKA.

Throughout the chapter we refer to the power-law radio spectral index α, defined in the sense that $S_\nu \propto \nu^{-\alpha}$. For a power-law electron energy distribution, $N(E) \propto E^{-p}$, the spectral index α is given

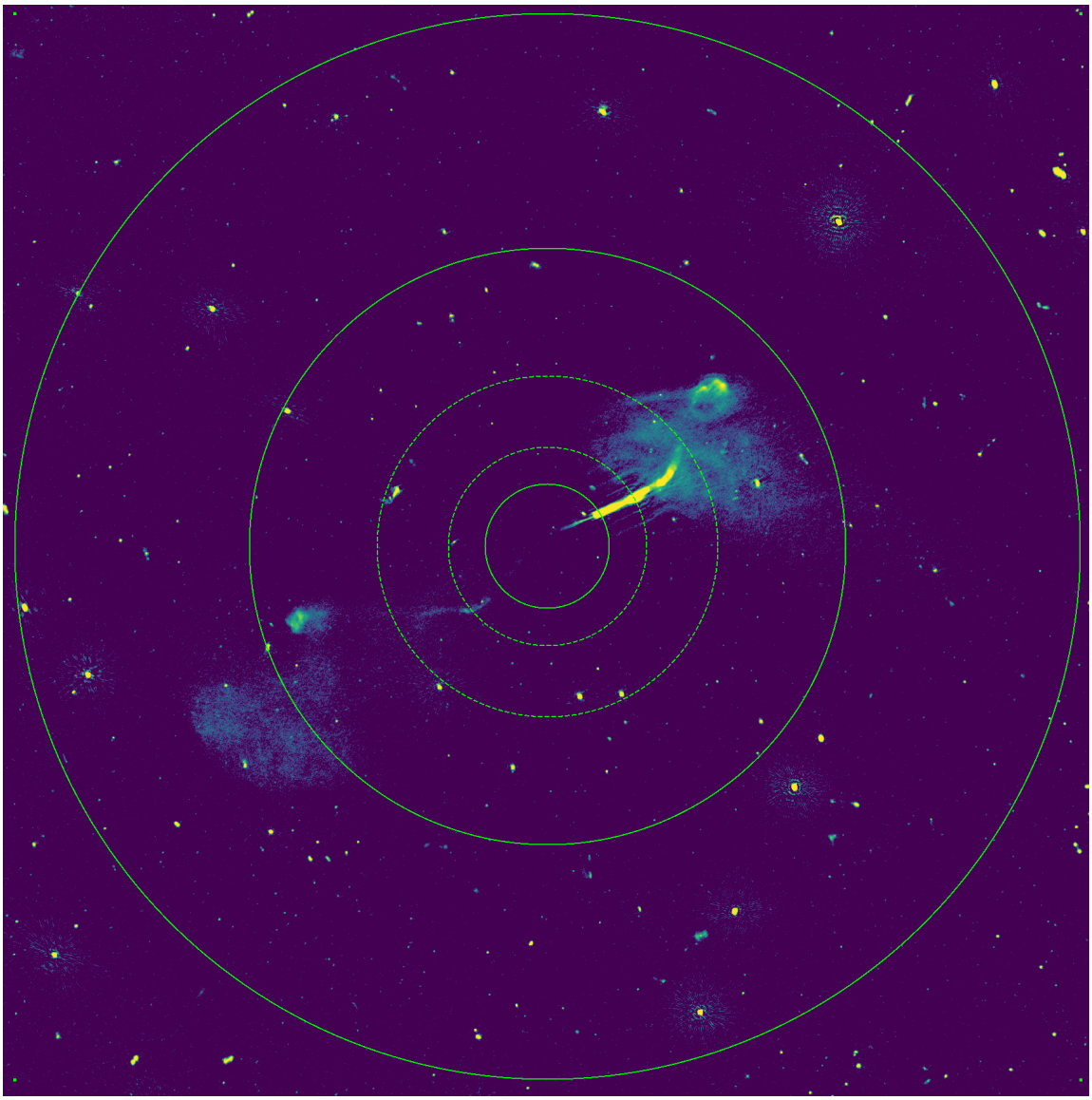

Figure 1: LOFAR (LoTSS: Shimwell et al. 2026) view of the nearby degree-scale radio galaxy NGC 6251 at 144 MHz with 6-arcsec resolution. Many other smaller radio galaxies can be seen in the same field. The image shows a $1.5° \times 1.5°$ field of view (FOV) matched to the FOV of SKA-Low at 300 MHz, the frequency at which Low will achieve the same resolution as LOFAR. Circles show, from largest to smallest, the FWHM FOV of Low at 300 MHz, which is similar to that of Mid band 1 at its central frequency, and the FOV of Mid bands 2, 3 and 4 (dotted lines as bands 3 and 4 will not be available initially), and 5a at their central frequencies. Observations of the largest sources will be increasingly restricted by the FOV and the shortest available baseline as they move to higher frequency and higher resolution.

by $\alpha = (p - 1)/2$.

2 Observations of radio galaxies with the SKA

As discussed above, radio galaxies are synchrotron emitters, which means that their radio emission is broad-band, extending in many cases from the lowest to highest frequencies available. Thus the entire frequency range from 50 MHz to 15 GHz offered by the SKA can be used for this type of work. However, resolution is a key limiting factor. As we will outline below, much of the insight into radio AGN physics comes from resolved studies of the population, and observations show (Sweijen et al., 2025) that the angular sizes of about half the studied population of radio galaxies in one LOFAR deep field with flux density > 0.6 mJy are less than a few arcsec. The resolution of SKA-Low (hereafter Low) will range from around 20 to around 3 arcsec across the band (from lowest to highest frequency) while that of SKA-Mid (hereafter Mid) will range from around 1.5 arcsec to 0.03 arcsec across bands 1-5. Thus it will only be possible to resolve the bulk of the population at the highest frequencies using Mid, while resolved studies with Low will tend to cover a luminous, physically large subset of targets. Wide-area surveys with Low (at the high-frequency end to avoid the confusion limit) should however allow the selection of a large population of AGN, with a sky density around 1000 deg^{-2} (Hardcastle et al., 2025). Because of its relatively small (few arcmin) field of view, Mid (particularly at band 5) will likely be most useful for targeted observations of individual objects or for deep surveys of smaller sky areas. The big gains in this area will come from the SKA's sensitivity and image fidelity compared to other facilities, which will enable us to build up observations of statistically meaningfully samples much more quickly than hitherto.

Physical size is also a factor. Powerful classical radio galaxies are often physically large, extending to scales of hundreds of kpc to Mpc scales (Laing et al., 1983; Bridle and Perley, 1984), and these sizes correspond to large angular sizes (Fig. 1). To image their extended structure and measure physical size and other parameters of their lobes, such as their Fanaroff-Riley classification (Fanaroff and Riley, 1974) arcsec-scale resolution is often sufficient, including at very low radio (~58 MHz) frequencies (Boxelaar et al., 2025), while the imaging of these largest-scale structures at high frequencies will be limited by the Mid primary beam and by the SKA's shortest baselines (which, however, are very short, of the order of twice the diameter of the individual antennas for Mid, meaning that structures of order half the primary beam in size can be imaged).

Radio galaxies all launch bipolar jets, but as is well known, their morphology is related to their luminosity: the most powerful objects tend to have a Fanaroff-Riley type II (FRII) morphology (Fanaroff and Riley, 1974; Fanaroff et al., 2021) showing faint or invisible emission related to the jets but bright hotspots at the end of well defined lobes, whereas in the classical Fanaroff-Riley class I (FRI) morphology bright inner jets feed into lobes or plumes. This morphological classification and its relationship to luminosity was based on low-sensitivity, low-fidelity observations of small samples of bright objects, and precursor work has shown us that we can expect objects that do not fit this pattern (Capetti et al., 2017; Mingo et al., 2019) as well as much more complication in the low-surface-brightness structures that will be revealed with the SKA. These classifications (or the structures responsible for them) most likely also evolve with redshift, something that can only be properly explored with the SKA.

Below we list some observational projects that will be enabled by the SKA's capabilities.

2.1 Distribution of source sizes and luminosities

As noted above, observations of the distributions of radio galaxies on the power-linear size (PD) plane are fundamental to the study of the life cycle of radio galaxies. Together with the evolving radio luminosity function, they provide the large-scale observational constraints on any model that links the radio AGN population to the accretion history of supermassive black holes and the evolution of their host galaxies. The SKA's potential contribution in this area was already discussed by Kapińska et al. (2014) and the reader is referred to that paper for further details. Here we just note that the change in design of the SKA relative to what was under consideration in 2014 does affect its capabilities in that area. Wide-area surveys with Low, as discussed above, will give an unrivalled deep view of the overall population, particularly when combined with EMU data at higher frequencies and with the deep optical data that will be available over the Southern hemisphere in the coming decades, and will allow the selection of sources for followup with Mid along the lines discussed further below. We can expect Low to see much the same range of luminosity of AGN as LOFAR currently does, i.e. between around 10^{21} and 10^{30} W Hz^{-1} at 150 MHz (Hardcastle et al., 2025) But we can no longer expect the wide-area surveys to give us sub-arcsec resolution over large areas, and so to resolve the bulk of the radio AGN population; objects smaller than 10-100 kpc (for a plausible distribution of redshifts) will remain unresolved with Low, and this constitutes a significant fraction, up to 80%, of an AGN sample (Hardcastle et al., 2025; Sweijen et al., 2025). Size and morphological information will need to be provided in the SKA1 era by a combination of observations with Mid over smaller fields and other instruments, such as LOFAR, or by VLBI. It is certainly possible to imagine a high-frequency survey with Mid that would give high resolution over intermediate areas — comparable, for example, to the tens of square degrees currently provided by the MeerKAT International GHz Tiered Extragalactic Exploration survey (MIGHTEE: Hale et al. 2025) but conducted at band 5a, where the resolution will be around 0.1 arcsec. Covering the 20° MIGHTEE sky area to the same depth as MIGHTEE but at band 5a, taking account of a typical synchrotron spectral index, would require a few hundred hours of Mid observing time, assuming that a sensitivity of 0.7 μJy beam^{-1} would be achieved over around 0.15 deg^2 in one hour. Such a survey would resolve the vast majority of radio AGN in the field (Sweijen et al., 2025) and would also greatly improve the ability to separate AGN emission from that due to star formation (cf. Morabito et al., 2022).

2.2 Spectral ageing studies

As a population of electrons in a radio galaxy radiates, higher-energy electrons radiate faster than lower-energy ones, which leads to a characteristic steepening of the radio spectrum (e.g. Jaffe and Perola, 1973). It has long been known that the synchrotron spectra of FRII radio galaxies systematically steepen with distance from the hot spots (Alexander and Leahy, 1987), while FRI radio galaxies show spectra that steepen with distance along the jets (Burch, 1977) and then, if lobes are present, with distance into the lobes as for FRIIs. The steepening is interpreted as evidence for 'synchrotron ageing', whereby the synchrotron energy loss process depletes high-energy electrons in the source as they move away from the acceleration site (Pacholczyk, 1970; Jaffe and Perola, 1973; Leahy, 1991). If we are really observing the effects of synchrotron ageing, and if the magnetic field strength is known, or can be estimated, e.g. from inverse-Compton observations (e.g Ineson

et al., 2017) then in principle resolved images of the radio spectra allow us to measure plasma age as a function of position in the source, which allows the determination of quantities like total source age and expansion speed, and also allows a timeline to be established for the source's phase(s) of activity. Different models of radiative loss make different predictions which can in principle be tested with a high-enough quality radio spectrum.

While broad-band radio observations have established the reality of spectral ageing at low frequencies (Lal and Rao, 2004, 2007; Sakelliou et al., 2008; Harwood et al., 2013; Jamrozy et al., 2008), high-frequency observations are important in this context because the spectral age probed by a frequency ν goes as $\nu^{-1/2}$. Thus, in principle, observations at the high end of frequency probe electrons an order of magnitude younger than those seen in the low end of frequency. Relative to existing studies with the VLA, GMRT or LOFAR, SKA spectral studies will be able to produce well-sampled, matched-resolution images across two decades in frequency for appropriately sized sources, due to the SKA's unrivalled (u, v) coverage. For compact, young sources, resolved spectral ageing studies are likely *only* to be possible with the high frequencies of Mid (e.g. Heesen et al., 2014), although these will need to be tied to low frequencies to estimate injection indices, and care will be needed to take account of low-frequency turnovers that are known to appear in higher frequencies in smaller sources (O'Dea and Baum, 1997) and which will require modelling in terms of free-free (e.g. Bicknell et al., 2018; Young et al., 2025) and/or synchrotron self-absorption.

Broad-band spectral studies have the capability to answer three key questions:

1. What are the spectra of aged regions? Are they consistent across a broad spectral range with theoretical models?

2. Are the spectral ages derived from detailed imaging consistent with dynamical ages derived from models of radio source expansion and observations of radio source environments?

3. Are the particles responsible for the low-frequency emission entirely co-spatial with those responsible for the high-frequency emission as seen in FRII radio galaxies?

The first of these questions is important because it gives insight into the micro-physics of the radio structures — in spite of many studies investigating this question, GHz-frequency work does not provide a definitive answer to the question of whether pitch-angle scattering is effective during loss as expected in the models of Jaffe and Perola (1973), for example (e.g. Harwood et al., 2013). High-resolution, high-fidelity, truly broad-band images should answer this by unambiguously locating the cutoff in the synchrotron spectrum at high energies if it exists, and maybe allow us to probe inhomogeneities in the magnetic field strengths as well (Tribble, 1993; Hardcastle, 2013).

Both the second and third questions are fundamental to the interpretation of spectral age measurements. The so-called 'spectral age problem' (Eilek, 1996) is the fact that spectral ages seem to be significantly younger than the expected dynamical ages where these can be modelled. Although the details of this discrepancy depend on factors like the unknown lobe magnetic field strength (and its history), the problem persists even when the best possible field strengths are used (Harwood et al., 2013; Mahatma et al., 2020). Possible solutions include mixing of plasma of different ages in the lobes (Turner et al., 2018; Jerrim et al., 2025), and/or *in situ* particle acceleration in the lobe, which

should be identifiable as a spectral *flattening* in certain parts of the lobes at high frequency (Lal and Rao, 2007). Existing low-resolution, low-sensitivity studies of small samples of lobes at high radio frequencies cannot test this model (Hardcastle and Looney, 2001) but SKA broad-band observations will enable us to establish the spectral properties of morphologically defined subsamples of RLAGN on a *statistical* rather than an individual basis. In addition to solving the spectral age problem and helping us to calibrate observed spectral ages as a constraint on radio source models, direct evidence for *in situ* leptonic particle acceleration in the lobes would give a previously unavailable insight into lobe micro-physics and might connect to models of the ultra-high-energy cosmic ray population (Hardcastle, 2010; Matthews et al., 2019).

With high sensitivity and image fidelity, it is now routine to fit spectral models to each individual pixel of an image of a source (Harwood et al., 2013), and the broader the frequency range available, the better the age constraints are. The key advance will be to build up systematic, consistent spectral age information for large samples. For example, Pinjarkar et al. (2023) used LOFAR, superMIGHTEE (upgraded GMRT; Lal et al., 2025) and MIGHTEE (MeerKAT) data at 144-1400 MHz to determine spectral ages for a sample of resolved sources in 3.5 deg^2 of the XMM-LSS deep field; but they were limited by their data to 10 arcsec resolution and to sources brighter than tens of mJy at 144 MHz. At the lowest-frequency end of Mid, where the resolution will be about 1.5 arcsec, a comparable deep-field survey could reach higher sensitivity within an hour. In band 5, one hour per pointing (covering several sources) would enable imaging of objects up to ten times fainter and six times smaller than those studied by Pinjarkar et al. (2023), providing matched-resolution coverage from 350 MHz to 15 GHz for a sample tens to hundreds of times larger than the current state of the art.

2.3 Magnetic fields and rotation measure in lobes

The radio emission from radio galaxies is always intrinsically polarized, with an intrinsic direction which gives information on the mean magnetic field direction along the line of sight, and a fractional polarization which reflects the degree to which magnetic fields are aligned versus tangled on scales much smaller than the beam. However, this is complicated by Faraday rotation due to thermal electrons, which can be in the halo of the Milky Way, in the local environment of the radio galaxy but external to it, or even internal to the lobes. Unresolved Faraday rotation structure in front of the lobes can give rise to depolarization (Burn, 1966), which is frequency-dependent since the angle of Faraday rotation goes as λ^2, but if the Faraday screen can be resolved then only rotation will be seen. Faraday rotation internal to the lobes due to internal thermal electrons will lead to depolarization, independent of resolution, at low frequencies ($\nu < c\sqrt{Cn_{\rm th}|B_\parallel|D}$, where $n_{\rm th}$ is the number density of thermal electrons, $B_\parallel$ is the magnetic field strength along the line of sight, D is the depth through the source and $C = 2.62 \times 10^{-13}$ T^{-1}).

If the interest is in studying the magnetic field structure internal to the lobes, then working at high frequencies (band 5) will offer both the highest resolution and the lowest Faraday effects. Past studies of individual objects or small samples at high frequency with instruments such as the un-upgraded VLA required many tens of hours to build up the uv coverage required through multiple configurations. A classic study of this type by Bridle et al. (1994) reached noise levels of 20 μJy beam^{-1} at 5 GHz and imaged polarization in a modest sample of quasars with 0.35-

arcsec resolution. A ten-minute observation in band 5a will achieve the same *surface brightness* sensitivity with a beam 7 times smaller in area and with superior image fidelity. This would allow the generation of samples large enough for robust comparisons with MHD simulations, as well as probing the small-scale field structure in jets and hotspots (see below).

However, there is also substantial information in the Faraday rotation and/or depolarization itself, and studying that requires us to go to lower frequencies. Faraday rotation from an external medium gives us information about the product of the thermal electron density and the magnetic field vector component along the line of sight: this means that even if the thermal electron density is reasonably uniform, the rotation measure can vary on small scales from point to point due to the turbulent field in the intergalactic medium (where the definition of 'small scales' depends on the poorly known MHD turbulence scales in the external medium). At frequencies and resolutions that are too low, sources can thus be completely depolarized by beam depolarization effects (O'Sullivan et al., 2023), but in between (at frequencies between hundreds of MHz and a few GHz for typical radio galaxy environmental conditions) the Faraday screen can be partly or wholly resolved (e.g. Guidetti et al., 2011; Baidoo et al., 2023) and there is a sweet spot where information can be extracted about the large-scale environment without the need for expensive X-ray observations (Jerrim et al., 2024; Stimpson et al., 2025). Mid in bands 1 and 2 will be good in particular for the large-scale structures of radio AGN in poor environments, where there are few useful probes of the thermal electron density. Broad-band polarimetry at these frequency ranges is hardly explored, but we can compare with the pre-upgrade VLA imaging used by Guidetti et al. (2011), where observations of duration of several hours with resolution of 1.5 arcsec and sensitivity of 25 μJy beam^{-1} over a 50-MHz channel were used. In SKA band 2, the same sensitivity but with twice the resolution would be achieved in a 5-minute observation, generating 16 images of the same channel width to give an in-band rotation measure constraint. Much finer channel spacing could of course be used for rotation measure synthesis. Observations at the lowest frequencies possible (Mid band 1 or Low) will give the best constraints on any internal thermal electron content, and should be carried out on large scales where the external Faraday rotation is low, though it will likely be challenging to distinguish from external depolarization (Tribble, 1991; Stimpson et al., 2025).

2.4 Particle acceleration locations in FRIs and FRIIs

Jets of FRI and FRII sources interact differently with their environments (Lal et al., 2008). It is generally believed that all jets start off highly relativistic, and hence supersonic with respect to their internal sound speed, but that FRI jets decelerate by entrainment of thermal material, either from stellar winds or from the external environment, which injects mass into the jet and so decelerates it by conservation of momentum (Bicknell, 1984; Laing and Bridle, 2002; Lal et al., 2010, 2013; Perucho et al., 2014). Dissipative processes once the jet becomes trans-sonic cause particle acceleration and brightening in the inner parts of the jet, typically 1-10 kpc for powerful sources such as 3C 31 (Laing and Bridle, 2002). By contrast, FRII jets are powerful enough to escape from their galactic environment without significant deceleration, and so remain supersonic until the end of the jet where they terminate in a jet termination shock. The bright radio emission at the ends of FRII sources, which originates in the forward and/or reverse shock associated with jet termination, is thought to be the site of particle acceleration in FRIIs.

In pre-SKA instruments, the particle acceleration locations in both types of object, which have structure on small scales, have been hard to study with high resolution and sensitivity, as instruments like the VLA do not provide in a single observation the long and short baselines needed to image hotspots and inner jets in the presence of bright diffuse emission from lobes and plumes. The SKA will be able to image these structures in bulk at high resolution and with polarization capabilities, probing models of particle acceleration physics. High-resolution images of these regions at multiple frequencies will probe the 'injection index', the spectral index of material injected at the hotspot, which is a crucial ingredient in models of spectral ageing, and test whether it is consistent with the expectation from shock models. Hotspots in particular appear to be transient features, which evolve on a short timescale compared to the lifetime of a source, and the detailed structure and spectral ageing history of multiple hotspots can shed light on models of jet precession (Horton et al., 2023). The morphology of jets and hotspots may also differ between low and high-power FRIIs. Jets propagating through thermal ambient medium (for normal radio galaxies) and non-thermal ambient medium (for the inner jets of episodic radio galaxies) may have subtle difference in injection indices, hotspot speeds and efficiency of particle acceleration that can only be studied with the high resolution and high sensitivity observations that will be available with the SKA. As with other cases, the SKA will be able to build up large samples of high-resolution images of such objects with very high speed compared to previous work. Hotspots of FRIIs, because these objects are generally distant, need sub-arcsec resolution to study sub-kpc structure, and so are good targets for observations at band 5. For example, Hardcastle et al. (1998) used observations of bright 3C sources at a typical frequency of 8 GHz and a resolution of 0.25 arcsec to measure properties of hotspots at a single frequency from maps with rms noise levels of tens of μJy beam^{-1}, accumulating a sample of around 50 objects, based on observations spanning many hours of observation and many years of time due to the VLA's configuration cycle. Using 5-minute snapshots in SKA band 5a, a sample ten times larger, with a sensitivity ten times higher and a resolution twice as good (plus in-band spectral index information), could be obtained in a two-day observing campaign after selection from a wide-area survey.

2.5 Jet speed and structure

The speed of relativistic jets can be measured by observations of Doppler boosting and, for polarimetric observations, aberration, if we assume that the jet and counterjet in a particular system are intrinsically identical. Observations of jet deceleration and velocity structure in FRI sources are a key piece of evidence for the standard model of the FRI/FRII difference, as mentioned above. The sensitive, high-resolution polarimetric observations needed to do this for small samples of FRIs with the VLA (Laing and Bridle, 2014) could be generalized to much larger samples with the SKA to enable the study of the dependence of the jet kinematics on the sources' environment, host galaxy properties and jet power, and hence test the entrainment model for jet kinematics in detail.

Understanding the kinematics of FRII jets is much harder because the jets are typically much fainter, unless strongly beamed, and counterjets (the Doppler-suppressed jet receding from us) are often not detected in available imaging. Constraints come from the distribution of jet sidedness (e.g. Wardle and Aaron, 1997) and jet prominence (e.g. Lal et al., 2008; Mullin and Hardcastle, 2009; Lal et al., 2010), which give beaming speed estimates corresponding to $0.5 < \beta < 0.8$, consistent

with the idea that these jets remain relativistic. However, these beaming speeds for jets (in terms of Lorentz factor, $\Gamma \sim 1.5$) are much lower than the corresponding speeds for cores ($\Gamma \sim 10$) or to the values directly measured from VLBI observations of bulk speeds in quasars ($\Gamma > 20$); yet there is no evidence of the energy dissipation that would be observed if the jets decelerated from bulk $\Gamma \sim 10$ to $\Gamma \sim 1.5$ on kpc scales. The generally accepted explanation for this is that the FRII jets have velocity structure, and that the material seen on large scales is a slow-moving 'sheath' around a fast jet core which may carry most of the energy[1]. As noted above, velocity structure is already seen in Doppler boosting analysis of FRI jets, but if this is the case, we might expect to see resolved structure in total intensity and polarization in the jets of FRIIs as well when observed at the highest available resolution, e.g. with SKA band 5b. In addition, such observations should have the image fidelity to image counterjets in many more objects than at present (the limiting factor is likely the image fidelity needed to pick out the counterjets in the presence of complex filamentary structure in the lobes, rather than raw sensitivity) which gives additional constraints on beaming. Observations of 3C 353, a nearby low-power FRII source (Swain et al., 1998) are consistent with such a model but only the SKA can give the combination of high ($\sim$ 100-pc) resolution and sensitivity to build up an unbiased sample for this kind of study.

3 Physics of Radio Galaxies: Episodic Radio Galaxies

Episodic jet forming activity of AGN is quite ubiquitous in the Universe (Schoenmakers et al., 2000; Saripalli et al., 2003; Saikia et al., 2006; Safouris et al., 2008; Konar et al., 2013; Konar and Hardcastle, 2013; Nandi et al., 2019; Saikia and Jamrozy, 2009; Mahatma et al., 2023; Morganti, 2024; Dabhade et al., 2025). If radio loud AGN are observed with two episodes, i.e., two pairs of lobes with a common core, they are called double-double radio galaxies. Similarly, objects with three pairs of lobes with a common core are called triple-double radio galaxies. Objects which host a very small inner double, often seen as a steep-spectrum core, and so are presumably an early phase of the evolution of a double-double radio galaxy, fall under the general label of episodic sources. Since they presumably trace the same underlying physics of an interruption in the jet energy supply (Section 1) we will use the terms episodic, double-double, and triple-double synonymously throughout this chapter. For the double-double radio galaxies, the younger lobes inflated by the re-started jets in the current episode and lying between the two older lobes of the previous episode are called the inner double. The outer older lobes are called the outer double. Fig 2 shows an example in which an inner double is embedded in the diffuse relic plasma of outer lobes created in the previous episode. The episodic behaviour does not have any known dependence on the host galaxy of the AGN (e.g. Mahatma et al., 2023). It is yet to be understood whether the host galaxy of the AGN has any role to play in deciding the timescale of the active and quiescent phases.

Episodic behaviour of the radio loud AGN is responsible for the production of remnant radio galaxies and restarted jets. A lot of information related to duty cycle and jet dynamics comes from the remnant lobes (or, relic lobes) and the restarted jets through spectral ageing analysis. In this section, we discuss the SKA's potential to improve studies of duty cycles and jet dynamics based

[1] Konar and Hardcastle (2013) argue independently that the observed physics of double-double radio galaxies requires that a highly relativistic jet persist out to the hotspots, consistent with the spine-sheath model.

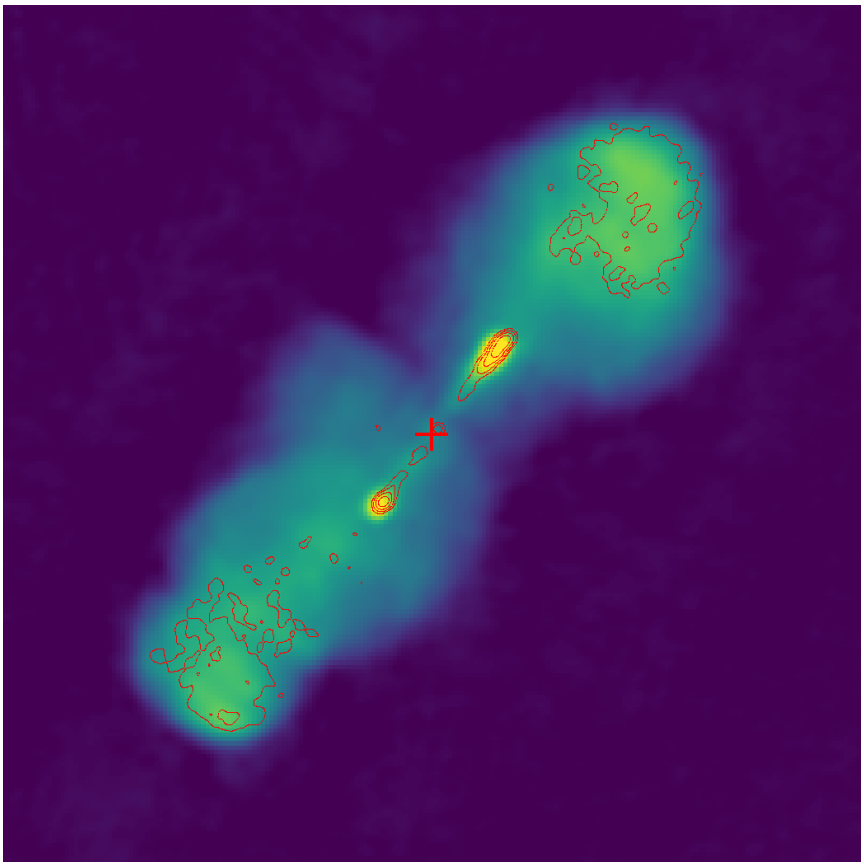

Figure 2: A double-double radio galaxy, J1158+2621 (4C 26.35), is shown in this image, which has a 5×5 arcmin field of view. The plus sign in red indicates the central position (11:58:20.1400, +26:21:12.00) of the optical host galaxy. The colour scale is the image from the LoTSS survey image data at 6 arcsec resolution while the contours are from the 1.4-GHz GMRT imaging of Konar et al. (2013), who carried out a detailed spectral ageing analysis. The contour levels are 1,2,4,8 mJy beam^{-1} for a resolution of 2.6 arcsec, while the logarithmic colour scale shows a lowest surface brightness of 1 mJy beam^{-1} with 6-arcsec beam at 144 MHz.

on episodic AGN. We defer our detailed discussion on remnant radio galaxies to Section 4.

3.1 What causes and controls jet activity in radio loud AGN?

As noted above and in Section 1, it is now clear that jet activity in radio loud AGN is episodic. The primary evidence for this comes from observations of the radio lobes created by a previous episode of jet activity (Schoenmakers et al., 2000; Lal et al., 2008). However, it is not clear a) what exactly causes the episodic behaviour, b) whether all radio loud AGN will exhibit the episodic activity, c) whether currently radio quiet AGN will some day start jet activity, d) whether the episodic jet activity is connected with a change of accretion state (low-hard and high soft states) as in stellar mass black hole binaries, and e) whether the feedback loop between supermassive black hole and thermal ambient medium can be causally connected to the episodic behaviour in jet activity. Addressing some of these questions needs X-ray, optical, mm (e.g., CO line) and cm (e.g. HI line) observations; however, radio observations with high resolution will definitely provide key information. For example, one of the crucial constraints for inferring the cause of episodic

radio galaxies is the range of observed duty cycle, as any model has to reproduce this in order to be considered successful. The duty cycle of jet activity, or jet duty cycle, is given by

$$\text{Jet duty cycle} = t_{\text{active}}/(t_{\text{active}} + t_{\text{quies}}), \quad (1)$$

where t_{active} and t_{quies} are the timescales of the active and quiescent phase of jet activity respectively. In the next section we consider how this can be constrained by radio observations.

3.2 What are the values of jet duty cycles for AGN?

Constraining jet duty cycle has been attempted only for a handful of sources by Konar et al. (2013) through spectral ageing analysis for FRII sources. They did not quote the values of the jet duty cycle as per the definition given above, but rather estimated the timescales of the active phase (t_{active}) and quiescent phase (t_{quies}) of jet activity. The jet duty cycle can thus in principle be estimated from their results for a handful of sources[2]. In addition, Konar et al. (2013) obtained only the upper and lower bounds on t_{innd}. The higher the resolution and sensitivity, the better we can constrain t_{innd} and hence the duty cycle, as we discuss below.

We can make use of spectral ageing analysis (Section 2.2) to constrain the age of the outer double (t_{outd}) and the age of the inner double (t_{innd}) and the time period of the quiescent phase (t_{quies}) of jet activity between two episodes. The formulae for timescale of active phase and quiescent phase derived by Konar et al. (2013) are

$$t_{\text{active}} = t_{\text{outd}} - (t_{\text{jet}} + t_{\text{ws}}) \quad (2)$$

and

$$t_{\text{quies}} = (t_{\text{ws}} + t_{\text{jet}}) - t_{\text{innd}} \quad (3)$$

respectively; where t_{active} and t_{quies} are the timescale of active and quiescent phase of the jet activity of the radio loud AGN respectively, t_{outd} and t_{innd} are the spectral ages of the inner and the outer doubles respectively, t_{jet} is the jet travel time of the radio emitting plasma for the outer double, and t_{ws} is the spectral age of the 'warm spot', i.e., the time elapsed between the moment when the last jet material was dumped at the outer hotspot (now the 'warm spot' at the end of the outer lobe) and the moment of observation.

Though Konar et al. (2013) had good estimates of t_{outd}, t_{jet} and t_{ws}, they had only limits on t_{innd}. This is because the integrated spectra of the inner doubles were power-laws within the observable range (few hundred MHz to around 8 or 15 GHz) in their observations to the accuracy permitted by their data. No curvature or breaks were observed in the integrated spectra of the inner doubles. Moreover, because of the limited resolution and sensitivity of the GMRT and JVLA, they could not estimate the ages at various parts of the lobes of the inner doubles of their samples, although this was possible for the outer lobes because of their larger size. Integrated spectra cannot give us accurate ages even if the curvature is detected, as the non-thermal plasma injected by the jets into

[2]These tend to be FRII sources because it is easier to identify the characteristic double-double morphology, although FRI sources can also be shown to be episodic in a few well-studied objects, such as the multiple outbursts seen in the nearest radio galaxy, Centaurus A (Morganti et al., 1999).

the lobes is injected at different times and with different values of the magnetic field strength (see also the discussion of the spectral age/dynamical age problem in Section 2.2).

The study of the inner lobes of episodic radio galaxies (e.g., double-double radio galaxies) will be much easier with the SKA. If the inner lobes can be imaged with sub-arcsecond resolution at several frequency bands from the lowest to the highest possible, the spectral ageing analysis will be greatly improved. The wide frequency coverage of the SKA along with its high sensitivity and resolution will greatly improve spectral ageing analyis, as discussed above (Section 2.2). For the inner doubles, although Konar et al. (2006), Konar et al. (2012), Konar et al. (2013) and Jamrozy et al. (2007) did not find any curvature in the integrated spectra of inner double of their sample sources, it is likely that curvature will be found for the spectra of the inner-lobe strips which are near the cores, which will help to constrain the ages of the inner doubles instead of giving limits on their ages. For some selected double-double radio galaxies like J1453+3308 (Konar et al., 2006), 4C29.30 (Jamrozy et al., 2007), J0116-4722 and J1158+2621 (Konar et al., 2013), the inner doubles will be well resolved at 1 arcsec or sub-arcsec resolution which will be available at frequencies higher than 500 MHz. That means that in all the Mid array bands the inner doubles of those sources will be well resolved and spectral ageing analysis in various strips of the inner lobes will be possible using the Mid array. Sensitivity will not be an issue at all. In J1453+3308 (Konar et al., 2006), we can see that in a 5-GHz image the backflow part of the lobes was detected down to a sensitivity level of 50 μJy beam^{-1}. As Mid in band 5 will reach μJy beam^{-1} noise levels in a ten-minute observation, all of the diffuse parts of the inner lobes are expected to be detected in a plausible SKA observing campaign. At frequencies lower than 5 GHz, the diffuse emission will be brighter, and hence is expected to be easily detected. At frequencies higher than 5 GHz, we cannot predict very firmly how much diffuse emission of the lobes will be detected, as the diffuse emission of the inner lobes is expected to suffer synchrotron losses. But irrespective of whether we can predict the diffuse emission at frequencies higher than 5 GHz, we can firmly state that spectral ageing analysis for various strips of the inner lobes, or even per pixel, will be possible with the help of the Mid array. Mid band 1 and Low will also be useful for spectral ageing analysis for the outer doubles and constraining the injection spectral indices of inner and outer doubles, for which we can use the integrated flux densities. Usually, we assume that the injection spectral index remains similar for the entire active phase of the jet activity. We can even afford to be skeptical about this assumption in the SKA era, however, as we can constrain the spectra of various strips of inner and outer lobes with higher sensitivity and/or carry out a pixel by pixel analysis. Thus, we can constrain the injection spectral index for many regions of the lobe separately and check if that is similar throughout the active phase of jet activity of radio galaxies. Since there will be good uv coverage for small baselines, the detection of diffuse emission for either the inner or outer doubles of double-double radio galaxies will not be an issue. There are already examples of variation of spectral injection spectral indices from one phase to the other in work by Brienza et al. (2020, 2021) and Rajpurohit et al. (2024). This may be due to variation of jet power over the lifetime of a single episode.

3.3 Hidden signatures of episodic activity in radio galaxies: relic lobes and steep spectrum cores

As noted above, radio galaxies are episodic and for FRII radio galaxies we can observe their episodes as multiple lobes, giving rise to a description of them as single double, double-double, triple double etc. The FRII radio galaxies which are observed as 'single doubles', i.e, only a single phase of activity is visible, are expected to cease their jet activity at some point in the future and be in a quiescent phase for some time before the restart their jet activity (see further below, Section 4). It is also plausible that something that now appears as a simple active radio galaxy might have finished its previous episode of jet activity so long ago that we do not observe the remnant lobes from a previous outburst as their surface brightness has dropped below the sensitivity level of the current radio telescopes. The work of searching for these remnant radio galaxies has already been started with the SKA precursor telescopes (see Brienza et al. (2017); Mahatma et al. (2018); Jurlin et al. (2020); Shabala et al. (2020) and many more) and a large number of candidate remnants have been discovered. With the SKA, with its extremely high surface brightness sensitivity, such large-scale diffuse emission around radio galaxies is expected to be discovered easily. As Kapińska et al. (2014) pointed out, there is a 'hidden world of secret lives of radio galaxies' that we can discover with instruments sensitive to low surface brightness, low-frequency emission. A preview of this is given by LOFAR, where we see several well-studied objects that show signatures of steep-spectrum, low-surface brightness emission interacting with the external medium (e.g. Hardcastle et al., 2019a; Brienza et al., 2021) but Low should give us many more, as Low will have a factor of 10 better sensitivity than LoTSS (and reach its confusion limit) with only 1 hour of integration time.

Another class of radio galaxies are those that show an unresolved but steep-spectrum or GPS core with the ordinary resolution of existing telescopes (in constrast to the flat-spectrum cores normally seen, which are the self-absorbed bases of the inner jets). With higher resolution sometimes these cores are resolved into mini-doubles, providing evidence for an additional epoch of jet activity that has only recently begun. An illustrative example of such a source is B0925+420, published by Brocksopp et al. (2007). They imaged this source with the 4.9 GHz and 8.4 GHz data both taken in VLA B-array. The innermost-double is clearly resolved with the VLA in both the 4.8 GHz and 8.4 GHz images, i.e. at arcsec resolution. Therefore, it will be worth investigating the steep spectrum cores of radio galaxies with the SKA. Godambe et al. (2009) investigated three relic sources, namely J0139+3957, J0200+4049 and J0807+7400, which have steep spectrum cores. The core spectrum of J0139+3957 is steeper at frequencies above 3 GHz, and gradually flattens to zero spectral index at lower frequencies. The core spectrum of J0200+4049 is steeper at frequencies above 1 GHz, and gradually flattens to zero and becomes slightly inverted at lower frequencies. These objects are therefore reminiscent of Giga-Hertz Peaked Spectrum (GPS) sources but exist inside large-scale lobes. The core of the other source J0807+7400 has also a steep spectral index between 300 MHz and 1.0 GHz. Beyond that it has a complicated spectrum: at lower frequencies than 300 MHz, there seems to be some absorption, while at frequencies higher than 1 GHz, the spectrum seems to be affected by variability. The highest resolution of their images was a few arcseconds and the cores were not resolved. Similar work in a larger sample, where prominent and steep spectrum cores have been interpreted as restarted activity, has been carried out by Nair et al. (2024). Many more such sources may be discovered with mini doubles inside the steep spectrum cores using the

SKA, which will have the ability to measure in-band spectral index at the same time as carrying out high-resolution imaging in a single band. Brocksopp et al. (2007) detected the diffuse lobe of the innermost double in the radio source B0925+420 with a sensitivity level of 22 μJy beam^{-1} in arcsec-resolution VLA observations. With an order of magnitude more sensitivity, as provided by Mid, many more inner doubles will be resolved. SKA VLBI studies along with SKA-Mid will greatly help to unravel the structure of the steep spectrum and GPS cores of radio galaxies.

3.4 The inner jet dynamics and ram pressure balance equation

In the context of astrophysical fluid dynamics, the dynamics of jets of radio galaxies describes the behavior of high-velocity flows through an ambient medium. A critical aspect of understanding these dynamics is the ram pressure balance equation, which governs the interaction between the jet and its surrounding environment. Ram pressure arises from the momentum flux of a fluid moving at high velocity relative to an object. In the context of jets, this pressure is exerted by the ambient medium on the jet as it propagates through it. Understanding ram pressure is essential for analyzing the confinement and collimation of jets, as it directly influences their structure and stability (Clarke and Carswell, 2007). The ram pressure balance equation is a fundamental principle that describes the equilibrium between the jet's momentum flux and the opposing pressure from the ambient medium. In a steady-state scenario, the non-relativistic equation can be written as

$$\dot{M} v_j^2 = P_{ram} A_h, \tag{4}$$

where $\dot{M}$ is the mass flow rate of the jet, v_j is the velocity of the jet, and A_h is the cross-sectional area of the jet head. This balance dictates the morphology and propagation speed of the jet, as it must counteract the external ram pressure to maintain its structure (Castorena et al., 2021)

Inner jets of double-double radio galaxies are ploughing through the relic radio plasma of outer lobes. Therefore, the inner lobe dynamics should be somewhat different from that of the outer lobes if thermal matter does not get entrained into the outer relic lobes of the episodic radio galaxies. Whether thermal matter has entrained into the outer relic lobes has to be studied through measurements of RM and/or depolarization (Section 2.3). Kaiser et al. (2000) used a ram pressure balance equation to estimate the jet-head (i.e., hotspot) speed ($v_{\rm h}$) through the ambient medium. They used a semi-relativistic equation which is

$$v_{\rm h} = \sqrt{\frac{Q_j}{c A_h \rho_a^0}} \tag{5}$$

where $Q_{\rm j}$ is the jet power, c is the speed of light, $A_{\rm h}$ is the jet head cross sectional area, and $\rho_{\rm a}^0$ is the rest mass density of the ambient medium. With the application of the above equation, Kaiser et al. (2000) attempted to predict that there must be thermal matter entrained into the relic lobes in order for hotspot formation to be possible. That is because too low an ambient medium density would make the jet head move with a speed close to the jet bulk speed. That would make the jet ballistic and no hotspot would be observed. Since we see the hotspots in the inner jets of double-double radio galaxies, according to Kaiser et al. (2000), there must be thermal matter entrained into the outer relic lobes. However, Konar and Hardcastle (2013) showed that the ram pressure balance

equation should be made fully relativistic to generalize this conclusion. The equation they derived is

$$\beta_{\rm h} = \left[\frac{1}{1+\sqrt{\frac{\beta_{\rm j} c A_{\rm h} w_{\rm a}}{Q_{\rm j}}}}\right] \tag{6}$$

where $\beta_{\rm h}$ and $\beta_{\rm j}$ are the hotspot speed and jet bulk speed in units of speed of light c, $A_{\rm h}$ is the jet-head cross section, $w_{\rm a}$ is the enthalpy density of the ambient medium, and $Q_{\rm j}$ is the jet power. Eq. 5 is a special case of eq. 6 in a non-relativistic situation, and hence eq. 6 is to be preferred, since we do not know from first principles whether the dynamics are relativistic. Konar and Hardcastle (2013) showed that even if there is no thermal matter entrainment and the non-thermal lobe plasma consists of electron-positron pair plasma (hereafter $e^- - e^+$ plasma) and the number density of pair plasma particles is in the range $10^{-9} - 10^{-8}$ cm^{-3}, hotspot formation is highly plausible. Therefore, the inner jet dynamics cannot tell us if thermal matter entrainment into the outer relic lobes has taken place or not. Instead, the measurement of RM internal to the lobes could tell us if such entrainment has occurred. Then one can apply the relativistic ram pressure balance equation from Konar and Hardcastle (2013) to study the inner jet dynamics of episodic radio galaxies.

As discussed in Section 2.3, Low may well be able to help us conclude if there is significant thermal matter entrainment into the outer relic lobes of episodic radio galaxies. If entrainment happens and we are able to obtain some estimates of the thermal matter density inside lobes, then that will be used to study the inner jet dynamics of episodic radio galaxies. Konar and Hardcastle (2013) used only non-thermal cocoon matter (no thermal matter) as the ambient medium for the inner jet propagation to estimate the jet-head speed and concluded that formation of hotspots at the jet-head of inner jets is quite plausible, and the jet-head speed has to be relativistic. However, this does not guarantee that there is no thermal matter inside the lobes. There can always be some amount of thermal matter which was entrained into the lobes. However, the amount of thermal matter inside the lobes cannot be very high (cf. Croston et al., 2018) as there is observational evidence for bow shock formation (see Fig.-6 of Konar and Hardcastle (2013) around the jet-head of inner jets propagating through the non-thermal cocoon matter of outer relic lobes. As Konar and Hardcastle (2013) argue, this is possible only if there is a jet termination shock at the inner jet-head and the jet head propagates with relativistic speed which is faster than the magnetosonic speed of the tenuous non-thermal ambient medium consisting of primarily non-thermal cocoon matter of the outer lobes. Because of the relativistic motion of the inner jet-heads, the radiation from the compact components of the jet-heads (which are due to jet termination shocks) undergoes relativistic boosting in the jet side and relativistic de-boosting in the counter-jet side. That makes the jet head in the jet side (which is moving towards us) appear as a prominent compact component suppressing the bow shock structure. Further, the jet head of the counter jet side loses the prominence of the compact component in the radiation because of the relavistic de-boosting effect and the bow shock becomes prominent. This, as pointed out by Konar and Hardcastle (2013), is a clear observational signature of the relativistic motion of the inner hotspots. Again with the SKA, because of very high resolution and sensitivity, for a large number of sources we will be able to detect the observational signatures of relativistic motion of the inner jet-heads. If, on the other hand, the inner jet-heads of some episodic radio galaxies may show strong compact components in the jet-heads of both jets and counter jets, this

will mean that the sufficient thermal matter entrainment into the relic outer lobes has taken place in those episodic radio galaxies to mean that the inner lobes no longer propagate at relativistic speeds. We will get a much better picture with the use of SKA data which will allow us to resolve the inner doubles.

3.5 Injection index and jet power

Konar and Hardcastle (2013) found that (i) the injection spectral indices of inner and outer doubles are quite similar in values within the error bars for a sample of 8 double-double radio galaxies, and (ii) there exists a correlation between injection spectral index and jet power for a sample of radio galaxies showing both single and double episodes together. This finding (ii) has triggered rethinking over the correlation between spectral index (α) and radio power at a given frequency (P_ν), and the correlation between spectral index (α) and redshift (z) as published by Laing and Peacock (1980) for a flux density limited sample. Since in a flux density limited sample the z and P_ν are correlated, $\alpha - P_\nu$ correlation can give rise to $\alpha - z$ correlation, and vice versa. Therefore, there has been a long-standing debate on which of these is the primary correlation (e.g. Blundell et al., 1999). Konar and Hardcastle (2013) and more recently Pinjarkar et al. (2025) revisited this discussion from the perspective of their particular observations. Konar and Hardcastle (2013) explained the similar injection index in the two episodes of double-double radio galaxies by introducing (a) strong shock at the hotspots of both inner and outer doubles along with spine-sheath structure of the jets with the spine moving with Lorentz factor $\Gamma_j > 10$, (b) similar jet power in two episodes with similar bulk Lorentz factor of the jet flow. To explain the correlation between injection spectral index ($\alpha_{\rm inj}$) and jet power ($Q_{\rm jet}$), they introduced the conjecture that higher jet power in sources is due to higher energy density in the jet fluid and not due to higher jet Lorentz factor. High energy density (likely to be in equipartition) will have higher magnetic field which enhances the synchrotron loss to steepen the originally produced injection index to a steeper value. Thus, higher jet power (or, higher monochromatic luminosity) will produce steeper observed injection spectral index. Thus Konar and Hardcastle (2013) interpreted that the correlation between spectral index (or, injection spectral index) and jet power is the primary correlation and one between spectral index (or, injection spectral index) and redshift is the secondary one. The latter correlation arises in a flux density limited sample because in such a sample there exists a correlation between redshift and radio power at a given frequency (or, monochromatic luminosity). In a recent study, Pinjarkar et al. (2025) found the evidence that the correlation between spectral index and luminosity is the primary correlation, which is in the line of the conclusion drawn by Konar and Hardcastle (2013) and supports original arguments by Blundell et al. (1999).

The above-mentioned results in (i) and (ii) give interesting constraints on AGN jet dynamics. With the SKA, the emission of inner and outer doubles will be clearly separated for many double-double radio galaxies for a wide range of frequencies starting from 350 MHz to 15 GHz in Mid. Verifying the correlation between the injection spectral indices of inner and outer doubles of double-double radio galaxies with a larger sample will be feasible with the advent of SKA. This will firmly establish if jet powers remain the same in each episode of episodic radio galaxies, or if this is a selection effect based on our existing small samples. In turn, that will provide an important constraint on models of the jet launching mechanism, jet dynamics and the cause of episodic jet activity in radio

loud AGN.

If detailed spectral ageing analysis is done for a large number of such sources with high resolution and sensitivity, we can also verify the correlation between injection spectral index and jet power. If verified, then we can even firmly establish that the correlation between spectral index and radio power is the primary correlation and the correlation between spectral index and redshift can arise because the radio power and spectral index are correlated in a flux limited sample. Given that the SKA will be highly sensitive, we can detect a large number of faint radio galaxies at higher redshifts over a broad range of frequencies. Therefore, we will be able to construct a sample up to a certain redshift such that all radio galaxies within that redshift will be detected in an SKA survey. The sample then will not be flux-density limited. We expect in such a situation that there will not be any correlation between redshift and radio power. In such a sample we must see the correlation between spectral index (or, injection spectral index) and jet power. This correlation will appear as the correlation between spectral index and radio power at given frequency (i.e., monochromatic luminosity). Hence the correlation between injection spectral index and jet power will be firmly established as the primary correlation. This would be best done in a deep field study like that of Pinjarkar et al. (2025), but with observations at comparable depths in all SKA bands to avoid the sensitivity-dependent biases in observable spectral index which affected that work. For example, extending the MIGHTEE fields used by Pinjarkar et al. (2025) to give good uniform sensitivity from Low to Mid band 5 frequencies could be done by the SKA in a few tens of hours.

3.6 Testable prediction

Konar and Hardcastle (2013) found similar injection spectral indices in two episodes in episodic radio galaxies. If this is due to similar jet power, as is their interpretation, their work suggests that in the population of radio galaxies, there is a significant fraction of strong radio galaxies which have similar jet power in two consecutive episodes. This in no way means that there are no sources with dissimilar jet power in two episodes. With the discovery of new sources with the SKA, we are hopeful to find a population of episodic radio galaxies with dissimilar injection spectral indices which would mean that some of those sources must have dissimilar jet powers in the two episodes. This would then allow an investigation of the factors that can change or preserve the jet power in different episodes. The underlying parameters responsible for preserving jet power in two episodes might be different in radiatively efficient and inefficient objects (LERGs and HERGs: Section 1) although both classes appear to be able to produce episodic radio galaxies. We might get clues to those underlying parameters, once detailed investigation of a statistically significant number of sources can be done through spectral ageing analysis combined with X-ray and optical studies as has been done by Konar et al. (2006), Konar et al. (2012), Konar et al. (2013), Jamrozy et al. (2007), Godambe et al. (2009), Konar and Hardcastle (2013), and Konar et al. (2019). From the work of Konar and Hardcastle (2013) and Konar et al. (2019), we can think of a few causes of dissimilar injection spectral indices in two episodes. We discuss them here. The injection spectral indices can be different in two episodes if (a) the black hole mass changes significantly from one episode to the other through matter accretion via radiatively efficient accretion in the radio quiet mode of AGN during a quiescent phase of jet activity, (b) the black hole spin changes due to angular momentum accumulation from the accreted matter, (c) the mode of accretion changes from radiatively efficient

to inefficient, or vice versa, irrespective of any change in black hole mass and spin, (d) the new jet activity is misaligned compared to the previous episode because of some large scale perturbation which may cause disturbance to the other underlying parameters deciding jet power, (e) the jet Lorentz factor changes significantly, or (f) the jet Lorentz factor is less than 10 so that the Mach number of the jet termination shock drastically varies in two episodes because of the diverse ambient medium density through which the jets propagate in two different episodes.

There may not be direct observable signatures for all the cause of dissimilar injection spectral indices in two episodes. However, one of our testable predictions is that we are likely to find dissimilar injection spectral indices in all or a large fraction of misaligned episodic radio galaxies. The episodic radio galaxy 3C 293 (Konar and Hardcastle, 2013) and the central radio galaxy of the cluster RBS 797 (Ubertosi et al., 2024) are illustrative examples of misaligned episodic radio galaxies with dissimilar injection spectral indices in two different episodes of jet activity. If through detailed spectral ageing analysis we can determine the spectral age and estimate the total energy budget of the lobes with equipartition assumption, then in principle we will be able to estimate the jet power for both pairs of lobes in episodic radio galaxies. If jet powers of inner and outer doubles in an episodic radio galaxy are the same, and still the injection spectral indices are dissimilar for two episodes; we can interpret the dissimilarity to be due to the Lorentz factor of the jet spine having a value less than 10 or so (see Konar and Hardcastle (2013)). If we measure highly dissimilar jet powers then we would expect to get dissimilar injection spectral indices in two episodes. Jet power differences can be due to various reasons which cannot always be distinguished through observations. With the advent of SKA with its high resolution and sensitivity, detailed spectral ageing studies of both inner and outer lobes will be possible and the picture of radio galaxy dynamics revealed by episodic sources will be much clearer than what it is today.

3.7 Lower-power and spiral-host episodic sources

As discussed above, most of our current understanding of jet duty cycles arises from multi-frequency spectral-aging studies of episodic radio galaxies hosted by elliptical galaxies. However, the phenomena of episodic radio jets at smaller linear scales can also be seen in nearby Seyfert galaxies. The galaxies Mrk 6, NGC2992 and NGC2639 have three episodes of radio jets/lobes each on different scales and different orientations to demonstrate their episodic nature (Rao et al., 2023) and references therein). These episodes are not as distinct as in episodic FRII radio galaxies. X-ray imaging studies of NGC 5813 shows three pairs of cavities clearly suggesting episodic non-thermal lobes pushing the thermal gas aside (Randall et al., 2011). A small but growing number of large radio galaxies have been identified in spiral or disk hosts. Since the earliest discoveries, the known sample of such systems has expanded to roughly three dozen (Ledlow et al., 1998; Yuan et al., 2024). Among these, three sources exhibit megaparsec-scale radio lobes with evidence of episodic activity — Speca (Hota et al., 2011), J23453268-0449256 (Bagchi et al., 2014) and LEDA 896325 (Sethi et al., 2025). Detailed investigations of these rare systems has remained limited, and it is yet to be established whether their properties differ systematically from those of giant episodic radio galaxies hosted by ellipticals. Given that the gaseous environments of spiral and elliptical galaxies differ markedly, the propagation of jets and expansion of radio lobes through these media are expected to have distinct implications for lobe energetics and radiative evolution. As the hosts

of these radio galaxies appear to have evolved primarily through passive processes rather than major mergers, assembling a larger sample including high-redshift source will be crucial for probing their cosmological evolution beyond $z = 2 - 3$ or "cosmic noon" (Florez et al., 2020). Future progress in this area will depend on sensitive, broad-band and wide-field observations with the SKA to identify additional disk-hosted episodic systems, complemented by high-resolution optical imaging (e.g. with *Euclid*) to confirm their spiral/disk host morphologies. The SKA will provide the sensitivity and resolution necessary to carry out spectral ageing studies of these faint radio sources with episodic jets out to cosmological distances.

4 Remnant radio galaxies, their identification and their characterization

4.1 Introduction to remnant radio galaxies

The jet activity of AGN in radio galaxies can persist for up to hundreds of Myr, during which the radio source can grow to sizes of a few hundred kiloparsecs and, in some cases, extend to megaparsec scales (Parma et al., 2007; Machalski et al., 2007; Pinjarkar et al., 2023). Once this active phase ends, the central engine either ceases activity or falls below the threshold required to sustain powerful jets, causing the outflows to shut down and the radio lobes to begin fading (Parma et al., 1999). This fading stage, referred to as the *remnant* or *dying* phase, is characterized by the disappearance of the radio core and jets, while the lobes remain detectable for several tens of Myr before becoming undetectable due to cumulative radiative and dynamical losses (Slee et al., 2001; Murgia et al., 2011; Lal, 2021). The remnant phase is generally thought to be much shorter than the preceding active phase, implying that remnant sources represent a brief terminal stage in the evolution of radio galaxies (Morganti, 2017). Consequently, remnant radio galaxies (hereafter remnants) are expected to be intrinsically rare, and their short lifetimes and low space densities mean that their physical properties and demographics remain poorly constrained.

Recent low-frequency studies have demonstrated that remnant radio emission can provide crucial constraints on the duty cycle of AGN jets. In particular, (Pandey-Pommier et al., 2016) used LOFAR MSSS and TGSS observations to detect relic lobes associated with previous activity cycles in nearby radio galaxies, highlighting how faint, diffuse emission traces earlier jet episodes that have ceased. Their spectral analysis revealed a correlation between the mean particle age of the relic emission and the central AGN properties, indicating that low-frequency relics preserve a record of past activity and can be used to infer the relative durations of active and quiescent phases. Such studies highlight the diagnostic potential of low-frequency observations for identifying dying or restarted radio galaxies. In addition to isolated radio galaxies, studies of brightest cluster galaxies in cool-core clusters reveal that recurrent jet activity plays a critical role in regulating the thermal state of the intracluster medium (Hamer et al., 2016). These observations indicate that AGN duty cycles are not only imprinted in relic lobes but also in the cumulative feedback energy deposited into the surrounding environment, highlighting the environmental dependence of episodic AGN activity.

To investigate the properties of remnants, several studies have conducted systematic searches, primarily utilizing low-frequency (<1.4 GHz) radio surveys (e.g. Parma et al., 2007; Murgia et al., 2011; Brienza et al., 2017; Godfrey et al., 2017; Mahatma et al., 2018; Jurlin et al., 2020; Dutta et al.,

2023). Low-frequency observations are particularly well suited for identifying remnants, as the synchrotron spectra of aged lobe plasma steepen significantly at higher frequencies. Consequently, samples of Ultra-Steep Spectrum (USS) radio sources have often been employed as efficient tracers of remnant candidates. However, simulations have clearly demonstrated that low-frequency (< 1 GHz) spectral selection is biased toward the oldest end of the remnant population and fails to identify younger remnants whose spectra have not yet steepened significantly (Brienza et al., 2017; Godfrey et al., 2017). Brienza et al. (2017) show that only a spectral selection that includes 5 GHz data — where spectral steepening is stronger and occurs more rapidly — can recover nearly the entire remnant population (up to 97%). In the absence of this, complementary morphological selection criteria become paramount.

Mahatma et al. (2018) applied a morphological approach, selecting remnants based on the absence of a radio core in sensitive high-frequency observations. These approaches are complicated by the fact that remnant dynamics depends on both progenitor and environment properties (Yates-Jones et al., 2023). However, using morphological and spectral criteria, core non-detection is inherently limited by observational sensitivity, and weak cores associated with either fading or rejuvenated AGN activity may still be present (Jurlin et al., 2021). Distinguishing between dying and restarted cores remains challenging, and there is evidence that low-level AGN activity may persist in massive galaxies regardless of evolutionary stage (see Sabater et al., 2019). Singh et al. (2021) and Dutta et al. (2023) employed both morphological and spectral criteria to assemble the largest sample of faint (8.0 mJy at 325 MHz) remnants identified to date, and this approach will need to be adopted in future SKA studies. The remnant fraction ($f_{\rm rem}$) is found to be only 5-8% even in deep radio fields, with the exact value depending on the flux density threshold at which the sources are probed (Jurlin et al., 2021; Lal, 2021; Dutta et al., 2023). Owing to their scarcity, the evolutionary pathways of radio galaxies during the remnant phase are not well understood, but if a selection strategy can be devised then the SKA should be able to find them in large numbers.

Shabala et al. (2020) used sensitive LOFAR samples of active and remnant radio galaxies from Jurlin et al. (2020) to place strong constraints on the distribution of jet lifetimes. Starting with a wide range of plausible progenitors with jet power and lifetime distributions constrained to be consistent with the observed active radio galaxy populations, these authors used a dynamical radio source model (Turner and Shabala, 2015) to predict the observable remnant fraction for each scenario. Their results showed that the overall population of radio galaxy jets has a pink noise-like power spectrum in age (Shabala et al., 2020); in other words, there are many more short-lived jets than long-lived ones. This requirement is placed by the relatively high (∼10%) observed remnant fraction (Turner and Shabala, 2015), and the rapid fading of remnant lobes (Turner and Shabala, 2020a). The SKA will be able to extend such work to larger samples, and definitively test the hints that the high-power radio galaxy population follows a different duty cycle to lower-power counterparts (Hardcastle et al., 2019b).

4.2 A case study of a remnant source in the COSMOS deep field

J095823+022628 serves as an example of a remnant radio galaxy in the COSMOS field, representative of the population of aged radio sources that upcoming SKA surveys are expected to uncover in large numbers, enabling detailed studies of their spectral evolution and energetics across cosmic

time. Morphologically, no radio core is detected in high-resolution imaging from MIGHTEE at 1284 MHz, superMIGHTEE (Lal et al., 2025) at 650 MHz, FIRST at 1.4 GHz, or VLASS at 3.0 GHz. This source also exhibits hotspot-like features in both lobes (see left panel of Figure 3), indicative of a relatively young remnant phase. The absence of a compact core in these datasets strongly supports its identification as a remnant. This source has also been examined by Vardoulaki et al. (2019, 2021), who used the more sensitive 1.4 GHz (Schinnerer et al., 2010) and 3.0 GHz VLA-COSMOS (Smolčić et al., 2017) surveys to identify the radio core. They detected a faint core with a core prominence ($S_{\rm core}/S_{\rm total}$) of $2{\times}10^{-3}$ (see middle panel of Figure 3). In the literature, remnant radio galaxies are typically characterised by very low core prominence values, generally in the range 10^{-4} to $3{\times}10^{-3}$ (see Brienza et al., 2017). The measured value for this source falls squarely within this range, supporting our interpretation that, morphologically, it satisfies the criteria for being a young remnant. In addition, the radio SED exhibits pronounced spectral curvature (see right panel of Figure 3), providing further evidence that J095823+022628 is a genuine remnant source. The potential optical host galaxy of this source (see middle panel of Figure 3) has a spectroscopic redshift of $z = 1.168 \pm 0.004$ (VIMOS; Lilly et al., 2023). The details of the spectral ageing analysis for this source are presented below.

Active radio galaxies typically exhibit a power-law injection radio spectrum in the location where particles are being injected. Over time, continuous radiative losses in the lobe plasma cause the spectrum to deviate from a simple power law, producing a spectral break. Because high-energy electrons lose energy more rapidly than low-energy ones, this break occurs at high frequencies, beyond which the spectrum steepens relative to the injection index ($\alpha_{\rm inj}$).

For active sources, the spectral shape is often reasonably well described by the continuous injection (CI) model ($\rm CI_{ON}$; Kardashev, 1962; Jaffe and Perola, 1973), which assumes a steady supply of relativistic plasma into the lobes over an active lifetime $t_{\rm active}$. In the remnant phase, once the jets switch off and no fresh particles are injected, the existing electron population continues to lose energy through radiative processes. This results in the formation of an additional spectral break at a higher frequency ($\nu_{\rm b,\ high}$) beyond the original injection break ($\nu_{\rm b,\ low}$). The lower break frequency, $\nu_{\rm b,\ low}$, represents the spectral steepening accumulated during the active phase, whereas $\nu_{\rm b,\ high}$ indicates the frequency above which the oldest electrons—those injected before the jet switched off—have largely expended their energy. The spectrum falls off exponentially beyond $\nu_{\rm b,\ high}$, and as the source ages, both $\nu_{\rm b,\ low}$ and $\nu_{\rm b,\ high}$ drift toward lower frequencies. The ratio of the two break frequencies encodes the relative duration of the remnant phase, expressed as

$$\frac{t_{\rm quies}}{t_{\rm s}} = \left(\frac{\nu_{\rm b,\ low}}{\nu_{\rm b,\ high}}\right)^{0.5}, \tag{7}$$

where $t_{\rm s} = t_{\rm active} + t_{\rm quies}$ is the total source age. For sufficiently old remnants, $\nu_{\rm b,\ high}$ approaches $\nu_{\rm b,\ low}$. The relation between the spectral age $t_{\rm s}$ and the observed break frequency $\nu_{\rm b}$ is given by (see Komissarov and Gubanov, 1994; Slee et al., 2001; Parma et al., 2007):

$$t_{\rm s} = 1590 \left[\frac{B_{\rm eq}^{0.5}}{(B_{\rm eq}^2 + B_{\rm CMB}^2)\sqrt{\nu_{\rm b}(1+z)}}\right] \ {\rm Myr}, \tag{8}$$

where $B_{\rm eq}$ is the equipartition magnetic field, $B_{\rm CMB} = 3.25(1{+}z)^2$ is the inverse Compton equivalent

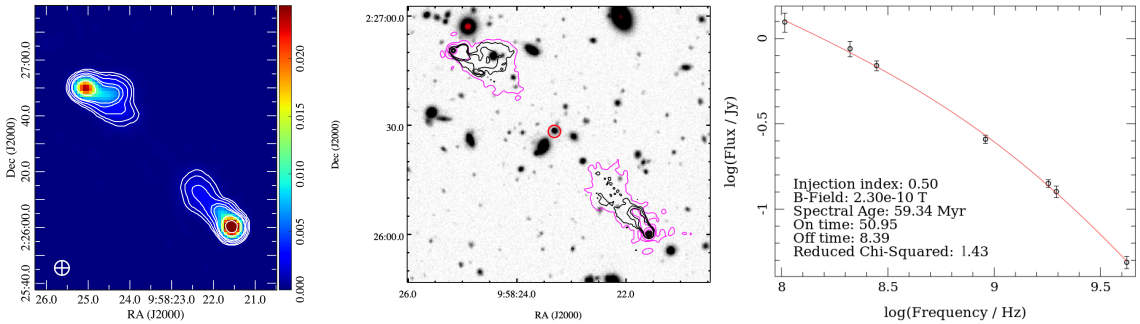

Figure 3: *Left panel:* MIGHTEE image of J095823+022628 in the COSMOS field with radio contours at $3\sigma \times (1, 2, 4, 8, 16, \ldots)$. *Middle panel:* 1.4 GHz VLA (in black) and 3.0 GHz VLA (in magenta) radio contours overlaid on the Ultra-VISTA NIR image, with the red circle marking the potential optical host. *Right panel:* Best-fitted radio SED of the source.

Table 1: Spectral ageing parameters for J095823+022628 obtained by using $\mathrm{CI_{OFF}}$ model.

Source Name	Redshift (z)	$\alpha_{\rm inj}$	B (μG)	$\nu_{\rm b,low}$ (MHz)	$\nu_{\rm b,high}$ (GHz)	$t_{\rm s}$ (Myr)	$t_{\rm active}$ (Myr)	$t_{\rm quies}$ (Myr)	$t_{\rm quies}/t_{\rm s}$
J095823+022628	1.168±0.004	0.50	2.3	564.97	5.38	$59.34^{+5.13}_{-5.32}$	$50.95^{+4.97}_{-5.12}$	$8.39^{+1.26}_{-1.45}$	$0.14^{+0.03}_{-0.03}$

magnetic field in units of μG and $\nu_{\rm b}$ is in GHz. This formulation accounts for radiative losses but neglects adiabatic expansion (English et al., 2019; Turner and Shabala, 2020a).

Spectral age estimates also require knowledge of the magnetic field strength. For this purpose, we adopted the equipartition magnetic field calculated using the PySynch[3] code (Hardcastle et al., 1998), and assumed magnetic field strength, $B = 0.4B_{\rm eq}$ (see Croston et al., 2005; Ineson et al., 2017; Mahatma et al., 2019). For this source, the magnetic field strength is estimated to be 2.3 μG ($B_{\rm eq}$ = 5.72 μG). In our modeling, we also used a constant injection index of $\alpha_{\rm inj}$ = 0.5, consistent with expectations for synchrotron emission from a power-law distribution of relativistic electrons.

To model the radio SED of our remnant source, we adopt the continuous injection-off model ($\mathrm{CI_{OFF}}$ or KGJP; Komissarov and Gubanov, 1994), which explicitly incorporates the remnant phase duration $t_{\rm quies}$ following the cessation of jet activity after an active phase of length $t_{\rm active}$. We constructed the radio SED using flux density measurements from 74 MHz VLSSr, 150 MHz TGSS, 200 MHz GLEAM, 650 MHz superMIGHTEE, 1284 MHz MIGHTEE, 1.4 GHz NVSS, and 3.0 GHz VLASS surveys. The parameters obtained using $\mathrm{CI_{OFF}}$ are given in Table 1 and the best-fitted radio SED is shown in the right panel of Figure 3. The total source age ($t_{\rm s}$) is estimated to be $59.34^{+5.13}_{-5.32}$ Myr, with an active phase duration ($t_{\rm active}$) of $50.95^{+4.97}_{-5.12}$ Myr and a remnant phase duration ($t_{\rm quies}$) of $8.39^{+1.26}_{-1.45}$ Myr. The ratio $t_{\rm quies}/t_{\rm s}$ further suggests that the source has spent only 14% of its lifetime in the remnant phase, consistent with its classification as a young remnant. Because the radio lobes fade on short timescales after the jets stop injecting energy, all observational searches are strongly biased toward detecting the youngest remnant sources (English et al., 2019; Shabala et al., 2024).

[3] https://github.com/mhardcastle/pysynch

4.3 Predictions with the SKA

As discussed in subsection 3.3 and 3.6, the SKA will revolutionize the detection and characterization of remnants. Its unprecedented sensitivity and resolution are expected to uncover a previously unexplored population of faint remnants residing at high redshifts. With Low covering the 50-350 MHz range and Mid spanning 0.35-15.4 GHz, these facilities will provide unprecedented spectral coverage for detailed modeling of aged electron populations in radio galaxies. Mid band 1 is expected to achieve an rms sensitivity of ~ 2 μJy beam^{-1} within one hour of integration (centered at 797.5 MHz), while Low will reach $\sim$ 12 μJy beam^{-1} at 200 MHz in the same time. The combination of large-area, deep, and multi-frequency surveys from the SKA and its pathfinders will thus enable the discovery of a statistically significant population of remnant radio galaxies spanning a wide range of evolutionary stages, providing transformative insights into the duty cycles and life histories of radio-loud AGN.

Using the MeerKAT $L-$band array with a 139.6 h observation in the COSMOS field, we achieved an rms sensitivity reaching down to ~ 2 μJy beam^{-1} and an angular resolution of ~ 6.0 arcsec. In contrast, the SKA will deliver an order-of-magnitude improvement in both sensitivity and survey speed, reaching sub-μJy levels with arcsecond-scale resolution in a fraction of the time. Such performance will revolutionize the study of remnant radio galaxies. Compared to current SKA pathfinders such as MeerKAT, uGMRT, LOFAR, and ASKAP, Mid is expected to increase the number of detectable remnant candidates by roughly a factor of 3-30 (point-source flux limit $S_{\rm lim,SKA} = S_{\rm lim,Old}/f$ and naive Euclidean source counts give $N \propto S^{-1.5}$, so $N_{\rm SKA}/N_{\rm Old} \approx f^{1.5}$), while Low could enhance detections by up to an order of 10-100, owing to its superior surface-brightness sensitivity to steep-spectrum, low-frequency emission. This improvement will enable comprehensive population studies of faint and extended remnants, providing unprecedented constraints on AGN duty cycles, spectral ageing, and the late evolutionary stages of radio galaxies.

5 Summary

The SKA will provide an unparalleled step forward in our understanding of radio galaxies, principally by providing very large samples of detailed images of objects that have hitherto been studied in such detail in very small samples or as single objects. We have emphasised in particular the resolution, sensitivity, and broad-band spectral capabilities of the Mid array in the possible projects that we have highlighted above, while not forgetting the contribution of Low to observations of steep-spectrum extended emission and low-frequency polarization/Faraday rotation studies. Much of the work described above can be done comensally with high-frequency surveys, together potentially with pointed large-sample studies for high-frequency work. All of it is well within the capabilities of the SKA AA4 array considered here. We can confidently expect a transformational improvement in our understanding of the radio galaxy population by the end of the coming decade.

References

P. Alexander and J. P. Leahy. *Mon. Not. R. Astron. Soc.*, 224:1, 1987.

A.-K. Baczko et al. In *Advancing Astrophysics with the SKA – II (AASKAII)*. 2026. arXiv search: Report number AASKAII/Baczko01.

J. Bagchi et al. *Astrophys. J.*, 788(2):174.1 – 174.18, June 2014. doi: 10.1088/0004-637X/788/2/174.

L. Baidoo et al. *Astrophys. J.*, 955(1):16, Sept. 2023. doi: 10.3847/1538-4357/acebc5.

R. D. Baldi et al. In *Advancing Astrophysics with the SKA – II (AASKAII)*. 2026. arXiv search: Report number AASKAII/Baldi01.

J. E. Baldwin. In D. S. Heeschen and C. M. Wade, editors, *Extragalactic Radio Sources*, volume 97 of *IAU Symposium*, pages 21–24, 1982.

P. N. Best and T. M. Heckman. *Mon. Not. R. Astron. Soc.*, 421:1569–1582, Apr. 2012. doi: 10.1111/j.1365-2966.2012.20414.x.

G. V. Bicknell. *Astrophys. J.*, 286:68–87, Nov. 1984. doi: 10.1086/162577.

G. V. Bicknell et al. *Mon. Not. R. Astron. Soc.*, 475(3):3493–3501, Apr. 2018. doi: 10.1093/mnras/sty070.

R. D. Blandford and R. L. Znajek. *Mon. Not. R. Astron. Soc.*, 179:433–456, May 1977. doi: 10.1093/mnras/179.3.433.

K. M. Blundell, S. Rawlings, and C. J. Willott. *Astron. J.*, 117(2):677–706, Feb. 1999. doi: 10.1086/300721.

J. M. Boxelaar et al. *arXiv e-prints*, art. arXiv:2509.15115, Sept. 2025. doi: 10.48550/arXiv.2509.15115.

A. H. Bridle and R. A. Perley. *Annu. Rev. Astron. Astrophys.*, 22:319, 1984.

A. H. Bridle et al. *Astron. J.*, 108:766, Sept. 1994. doi: 10.1086/117112.

M. Brienza et al. *Astron. Astrophys.*, 606:A98, Oct. 2017. doi: 10.1051/0004-6361/201730932.

M. Brienza et al. *A&A*, 638(A29):A29.1 – A29.14, Jun 2020. doi: 10.1051/0004-6361/202037457.

M. Brienza et al. *Nature Astronomy*, 5:1261–1267, Dec. 2021. doi: 10.1038/s41550-021-01491-0.

C. Brocksopp, C. R. Kaiser, A. P. Schoenmakers, and A. G. de Bruyn. *Mon. Not. R. Astron. Soc.*, 382:1019 – 1028, Dec. 2007. doi: 10.1111/j.1365-2966.2007.12483.x.

G. R. Burbidge. *Astrophys. J.*, 124:416, Sept. 1956. doi: 10.1086/146237.

S. F. Burch. *Mon. Not. R. Astron. Soc.*, 180:623, 1977.

B. J. Burn. *Mon. Not. R. Astron. Soc.*, 133:67, Jan. 1966. doi: 10.1093/mnras/133.1.67.

A. Capetti, F. Massaro, and R. D. Baldi. *Astron. Astrophys.*, 601:A81, May 2017. doi: 10.1051/0004-6361/201630247.

J. I. Castorena et al. *RMxAA*, 57:297 – 309, Apr. 2021. doi: doi:10.22201/ia.01851101p.2021.57.02.04.

C. J. Clarke and R. Carswell. *Principles of Astrophysical Fluid Dynamics*. Cambridge University Press, New york, 2007.

J. J. Condon, W. D. Cotton, and J. J. Broderick. *Astron. J.*, 124(2):675–689, Aug. 2002. doi: 10.1086/341650.

J. H. Croston et al. *Astrophys. J.*, 626(2):733–747, June 2005. doi: 10.1086/430170.

J. H. Croston, J. Ineson, and M. J. Hardcastle. *Mon. Not. R. Astron. Soc.*, 476(2):1614–1623, May 2018. doi: 10.1093/mnras/sty274.

P. Dabhade et al. *A&A*, 696(id.A97):A97.1 – A97.22, Apr. 2025. doi: 10.1051/0004-6361/202451918.

S. Dutta et al. *Astrophys. J.*, 944(2):176, Feb. 2023. doi: 10.3847/1538-4357/acaf01.

D. Eckert et al. *Galaxies*, 12(3):24, May 2024. doi: 10.3390/galaxies12030024.

J. A. Eilek. In Hardee P.E., Bridle A.H., Zensus J.A., editor, *Energy Transport in Radio Galaxies and Quasars*, page 281. ASP Conference Series vol. 100, San Francisco, 1996.

W. English, M. J. Hardcastle, and M. G. H. Krause. *Mon. Not. R. Astron. Soc.*, 490(4):5807–5819, Dec. 2019. doi: 10.1093/mnras/stz2978.

A. C. Fabian. *Annu. Rev. Astron. Astrophys.*, 50:455–489, Sept. 2012. doi: 10.1146/annurev-astro-081811-125521.

B. Fanaroff et al. *Mon. Not. R. Astron. Soc.*, 505(4):6003–6016, Aug. 2021. doi: 10.1093/mnras/stab1540.

B. L. Fanaroff and J. M. Riley. *Mon. Not. R. Astron. Soc.*, 167:31P–36P, May 1974. doi: 10.1093/mnras/167.1.31P.

J. Florez et al. *Mon. Not. R. Astron. Soc.*, 497(3):3273–3296, Sept. 2020. doi: 10.1093/mnras/staa2200.

S. Godambe, C. Konar, D. J. Saikia, and P. J. Wiita. *Mon. Not. R. Astron. Soc.*, 396:860 – 869, June 2009. doi: 10.1111/j.1365-2966.2009.14494.x.

L. E. H. Godfrey, R. Morganti, and M. Brienza. *Mon. Not. R. Astron. Soc.*, 471(1):891–907, Oct. 2017. doi: 10.1093/mnras/stx1538.

D. Guidetti et al. *Mon. Not. R. Astron. Soc.*, 413(4):2525–2544, June 2011. doi: 10.1111/j.1365-2966.2011.18321.x.

C. L. Hale et al. *Mon. Not. R. Astron. Soc.*, 536(3):2187–2211, Jan. 2025. doi: 10.1093/mnras/stae2528.

S.-L. Hamer, M. Pandey-Pommier, A.-C. Edge, and F. Combes. *SF2A-2016: Proceedings of the Annual meeting of the French Society of Astronomy and Astrophysics*, pages 385–389, Dec. 2016.

M. Hardcastle. *Nature Astronomy*, 2:273–274, Apr. 2018a. doi: 10.1038/s41550-018-0424-1.

M. J. Hardcastle. *Mon. Not. R. Astron. Soc.*, 405:2810–2816, July 2010. doi: 10.1111/j.1365-2966.2010.16668.x.

M. J. Hardcastle. *Mon. Not. R. Astron. Soc.*, 433(4):3364–3372, Aug. 2013. doi: 10.1093/mnras/stt1024.

M. J. Hardcastle. *Mon. Not. R. Astron. Soc.*, 475:2768–2786, Apr. 2018b. doi: 10.1093/mnras/stx3358.

M. J. Hardcastle and J. H. Croston. *New Astron. Rev.*, 88:101539, June 2020. doi: 10.1016/j.newar.2020.101539.

M. J. Hardcastle and L. W. Looney. *Mon. Not. R. Astron. Soc.*, 320:355, 2001.

M. J. Hardcastle, P. Alexander, G. G. Pooley, and J. M. Riley. *Mon. Not. R. Astron. Soc.*, 296(2):445–462, May 1998. doi: 10.1046/j.1365-8711.1998.01480.x.

M. J. Hardcastle, D. A. Evans, and J. H. Croston. *Mon. Not. R. Astron. Soc.*, 376(4):1849–1856, Apr. 2007. doi: 10.1111/j.1365-2966.2007.11572.x.

M. J. Hardcastle et al. *Mon. Not. R. Astron. Soc.*, 488(3):3416–3422, Sept. 2019a. doi: 10.1093/mnras/stz1910.

M. J. Hardcastle et al. *Astron. Astrophys.*, 622:A12, Feb 2019b. doi: 10.1051/0004-6361/201833893.

M. J. Hardcastle et al. *Mon. Not. R. Astron. Soc.*, 539(2):1856–1878, May 2025. doi: 10.1093/mnras/staf622.

J. J. Harwood, M. J. Hardcastle, J. H. Croston, and J. L. Goodger. *Mon. Not. R. Astron. Soc.*, 435

(4):3353–3375, Nov. 2013. doi: 10.1093/mnras/stt1526.

V. Heesen et al. *Mon. Not. R. Astron. Soc.*, 439(2):1364–1380, Apr. 2014. doi: 10.1093/mnras/stu043.

M. A. Horton, M. G. H. Krause, and M. J. Hardcastle. *Mon. Not. R. Astron. Soc.*, 499(4):5765–5781, Dec. 2020. doi: 10.1093/mnras/staa3020.

M. A. Horton, M. G. H. Krause, and M. J. Hardcastle. *Mon. Not. R. Astron. Soc.*, 521(2):2593–2606, May 2023. doi: 10.1093/mnras/stad674.

A. Hota et al. *Mon. Not. R. Astron. Soc.*, 417(1):L36 – L40, Oct. 2011. doi: 10.1111/j.1745-3933.2011.01115.x.

J. Ineson, J. H. Croston, M. J. Hardcastle, and B. Mingo. *Mon. Not. R. Astron. Soc.*, 467(2):1586–1607, May 2017. doi: 10.1093/mnras/stx189.

W. J. Jaffe and G. C. Perola. *Astron. Astrophys.*, 26:423, Aug. 1973.

M. Jamrozy et al. *Mon. Not. R. Astron. Soc.*, 378:581 – 593, June 2007. doi: 10.1111/j.1365-2966.2007.11782.x.

M. Jamrozy, C. Konar, and D. Machalski J., Saikia. *Mon. Not. R. Astron. Soc.*, 385(3):1286–1296, Apr. 2008. doi: 10.1111/j.1365-2966.2007.12772.x.

L. Jerrim et al. *arXiv e-prints*, art. arXiv:2510.16705, Oct. 2025. doi: 10.48550/arXiv.2510.16705.

L. A. Jerrim et al. *Mon. Not. R. Astron. Soc.*, 531(2):2532–2550, June 2024. doi: 10.1093/mnras/stae1317.

N. Jurlin et al. *Astron. Astrophys.*, 638:A34, June 2020. doi: 10.1051/0004-6361/201936955.

N. Jurlin et al. *Astron. Astrophys.*, 653:A110, Sept. 2021. doi: 10.1051/0004-6361/202040102.

C. R. Kaiser, J. Dennett-Thorpe, and P. Alexander. *Mon. Not. R. Astron. Soc.*, 292(3):723–732, Dec. 1997. doi: 10.1093/mnras/292.3.723.

C. R. Kaiser, A. P. Schoenmakers, and R. H. J. A. *Mon. Not. R. Astron. Soc.*, 315:381 – 394, June 2000. doi: 10.1046/j.1365-8711.2000.03431.x.

A. D. Kapińska et al. Advancing astrophysics with the square kilometre array (aaska14), 2014.

N. S. Kardashev. *Soviet Ast.*, 6:317, Dec. 1962.

S. S. Komissarov and A. G. Gubanov. *Astron. Astrophys.*, 285:27–43, May 1994.

C. Konar and M. J. Hardcastle. *Mon. Not. R. Astron. Soc.*, 436(2):1595–1614, Dec. 2013. doi: 10.1093/mnras/stt1676.

C. Konar, D. J. Saikia, M. Jamrozy, and J. Machalski. *Mon. Not. R. Astron. Soc.*, 372:693 – 702, Oct. 2006. doi: 10.1111/j.1365-2966.2006.10874.x.

C. Konar et al. *Mon. Not. R. Astron. Soc.*, 424:1061 – 1076, Aug. 2012. doi: 10.1111/j.1365-2966.2012.21279.x.

C. Konar, M. J. Hardcastle, M. Jamrozy, and J. H. Croston. *Mon. Not. R. Astron. Soc.*, 430:2137 – 2153, Apr. 2013. doi: 10.1093/mnras/stt040.

C. Konar et al. *Mon. Not. R. Astron. Soc.*, 486:3975 – 3991, July 2019. doi: 10.1093/mnras/stz1089.

M. G. H. Krause et al. *Mon. Not. R. Astron. Soc.*, 482:240–261, Jan. 2019. doi: 10.1093/mnras/sty2558.

R. A. Laing and A. H. Bridle. *Mon. Not. R. Astron. Soc.*, 336(4):1161–1180, Nov. 2002. doi: 10.1046/j.1365-8711.2002.05873.x.

R. A. Laing and A. H. Bridle. *Mon. Not. R. Astron. Soc.*, 437(4):3405–3441, Feb. 2014. doi: 10.1093/mnras/stt2138.

R. A. Laing and J. A. Peacock. *Mon. Not. R. Astron. Soc.*, 190:903 – 924, Mar. 1980. doi: 10.1093/mnras/190.4.903.

R. A. Laing, J. M. Riley, and M. S. Longair. *Mon. Not. R. Astron. Soc.*, 204:151, 1983.

D. V. Lal. *Astrophys. J.*, 915(2):126, July 2021. doi: 10.3847/1538-4357/ac042d.

D. V. Lal and A. P. Rao. *Astron. Astrophys.*, 420:491–499, Jun 2004. doi: 10.1051/0004-6361:20035777.

D. V. Lal and A. P. Rao. *Mon. Not. R. Astron. Soc.*, 374(3):1085–1102, Jan 2007. doi: 10.1111/j.1365-2966.2006.11225.x.

D. V. Lal, M. J. Hardcastle, and R. P. Kraft. *Mon. Not. R. Astron. Soc.*, 390(3):1105–1116, Nov. 2008. doi: 10.1111/j.1365-2966.2008.13810.x.

D. V. Lal et al. *Astrophys. J.*, 722(2):1735–1743, Oct. 2010. doi: 10.1088/0004-637X/722/2/1735.

D. V. Lal et al. *Astrophys. J.*, 764(1):83, Feb. 2013. doi: 10.1088/0004-637X/764/1/83.

D. V. Lal et al. *Astrophys. J.*, 991(1):9, Sept. 2025. doi: 10.3847/1538-4357/adf6dc.

J. P. Leahy. In Hughes P.A., editor, *Beams and Jets in Astrophysics*, page 100. Cambridge University Press, Cambridge, 1991.

M. J. Ledlow, F. N. Owen, and W. C. Keel. *Astrophys. J.*, 495(1):227 – 238, Mar. 1998. doi: 10.1086/305251.

S. J. Lilly et al. VizieR Online Data Catalog: zCOSMOS-bright catalog, DR3 (Lilly+, 2007). VizieR On-line Data Catalog: J/ApJS/172/70. Originally published in: 2007ApJS..172...70L, June 2023.

J. Machalski, K. T. Chyży, Ł. Stawarz, and D. Kozieł. *Astron. Astrophys.*, 462(1):43–55, Jan. 2007. doi: 10.1051/0004-6361:20066121.

M. Magliocchetti. *Astron. Astrophys. Rev.*, 30(1):6, Dec. 2022. doi: 10.1007/s00159-022-00142-1.

V. H. Mahatma et al. *Mon. Not. R. Astron. Soc.*, 475(4):4557–4578, Apr. 2018. doi: 10.1093/mnras/sty025.

V. H. Mahatma et al. *Astron. Astrophys.*, 622:A13, Feb. 2019. doi: 10.1051/0004-6361/201833973.

V. H. Mahatma et al. *Mon. Not. R. Astron. Soc.*, 491(4):5015–5034, Feb. 2020. doi: 10.1093/mnras/stz3396.

V. H. Mahatma et al. *Mon. Not. R. Astron. Soc.*, 520(3):4427 – 4442, Apr. 2023. doi: 10.1093/mnras/stad395.

J. H. Matthews, A. R. Bell, K. M. Blundell, and A. T. Araudo. *Mon. Not. R. Astron. Soc.*, 482(4):4303–4321, Feb 2019. doi: 10.1093/mnras/sty2936.

B. R. McNamara and P. E. J. Nulsen. *New Journal of Physics*, 14(5):055023, May 2012. doi: 10.1088/1367-2630/14/5/055023.

D. Merritt and R. D. Ekers. *Science*, 297:1310–1313, Aug. 2002. doi: 10.1126/science.1074688.

B. Mingo et al. *Mon. Not. R. Astron. Soc.*, 440:269–297, May 2014. doi: 10.1093/mnras/stu263.

B. Mingo et al. *Mon. Not. R. Astron. Soc.*, 488(2):2701–2721, Sept. 2019. doi: 10.1093/mnras/stz1901.

L. K. Morabito et al. *Mon. Not. R. Astron. Soc.*, 515(4):5758–5774, Oct. 2022. doi: 10.1093/mnras/stac2129.

R. Morganti. *Nature Astronomy*, 1:596–605, Sept. 2017. doi: 10.1038/s41550-017-0223-0.

R. Morganti. *Galaxies*, 12(2):11.1 – 11.16, Mar. 2024. doi: 10.3390/galaxies12020011.

R. Morganti, N. E. B. Killeen, R. D. Ekers, and T. A. Oosterloo. *Mon. Not. R. Astron. Soc.*, 307(4):

750–760, Aug. 1999. doi: 10.1046/j.1365-8711.1999.02622.x.

R. I. J. Mostert et al. *Astron. Astrophys.*, 691:A185, Nov. 2024. doi: 10.1051/0004-6361/202348897.

L. M. Mullin and M. J. Hardcastle. *Mon. Not. R. Astron. Soc.*, 398(4):1989–2004, Oct. 2009. doi: 10.1111/j.1365-2966.2009.15232.x.

M. Murgia et al. *Astron. Astrophys.*, 526:A148, Feb. 2011. doi: 10.1051/0004-6361/201015302.

D. G. Nair et al. *A&A*, 691(A287):A287.1 – A287.19, Nov 2024. doi: 10.1051/0004-6361/202451522.

S. Nandi et al. *Mon. Not. R. Astron. Soc.*, 486(4):5158 – 5170, July 2019. doi: 10.1093/mnras/stz1184.

R. Narayan and I. Yi. *Astrophys. J.*, 452:710 – 735, Oct. 1995. doi: 10.48550/arXiv.astro-ph/9411059.

C. P. O'Dea and S. A. Baum. *Astron. J.*, 113:148–161, Jan. 1997. doi: 10.1086/118241.

M. S. S. L. Oei et al. *Nature*, 633(8030):537–541, Sept. 2024. doi: 10.1038/s41586-024-07879-y.

S. P. O'Sullivan et al. *Mon. Not. R. Astron. Soc.*, 519(4):5723–5742, Mar. 2023. doi: 10.1093/mnras/stac3820.

A. G. Pacholczyk. *Radio Astrophysics*. Freeman, San Francisco, 1970.

M. Pandey-Pommier, H. Intema, and G. Heald. *SF2A-2016: Proceedings of the Annual meeting of the French Society of Astronomy and Astrophysics*, pages 379–383, Dec. 2016.

F. Panessa et al. In *Advancing Astrophysics with the SKA – II (AASKAII)*. 2026. arXiv search: Report number AASKAII/Panessa01.

P. Parma et al. *Astron. Astrophys.*, 344:7–16, Apr. 1999.

P. Parma et al. *Astron. Astrophys.*, 470(3):875–888, Aug. 2007. doi: 10.1051/0004-6361:20077592.

M. Perucho, J. M. Martí, R. A. Laing, and P. E. Hardee. *Mon. Not. R. Astron. Soc.*, 441(2):1488–1503, June 2014. doi: 10.1093/mnras/stu676.

S. Pinjarkar et al. *Mon. Not. R. Astron. Soc.*, 523(1):620–639, July 2023. doi: 10.1093/mnras/stad1432.

S. Pinjarkar et al. *Mon. Not. R. Astron. Soc.*, 537:3481 – 3498, Mar. 2025. doi: 10.1093/mnras/staf209.

K. Rajpurohit et al. *Astrophys. J.*, 976(1):64.1 – 64.21, nov 2024. doi: 10.3847/1538-4357/ad8136.

S. W. Randall et al. *Astrophys. J.*, 726(2):86.1 – 86.18, Jan. 2011. doi: doi:10.1088/0004-637X/726/2/86.

V. V. Rao et al. *Mon. Not. R. Astron. Soc.*, 524(2):1615–1624, June 2023. doi: 10.1093/mnras/stad1901.

J. Sabater et al. *Astron. Astrophys.*, 622:A17, Feb. 2019. doi: 10.1051/0004-6361/201833883.

V. Safouris, R. Subrahmanyan, G. V. Bicknell, and L. Saripalli. *Mon. Not. R. Astron. Soc.*, 385(4):2117 – 2135, Apr. 2008. doi: 10.1111/j.1365-2966.2008.12975.x.

D. J. Saikia and M. Jamrozy. *Mon. Not. R. Astron. Soc.*, 37:63 – 89, Sept. 2009.

D. J. Saikia, C. Konar, and V. K. Kulkarni. *Mon. Not. R. Astron. Soc.*, 366(4):1391 – 1398, Mar. 2006. doi: 10.1111/j.1365-2966.2005.09926.x.

I. Sakelliou, M. J. Hardcastle, and N. N. Jetha. *Mon. Not. R. Astron. Soc.*, 384:87, 2008.

L. Saripalli, R. Subrahmanyan, and N. Udaya Shankar. *Astrophys. J.*, 590(1):181 – 191, June 2003. doi: 10.1086/375004.

E. Schinnerer et al. *Astrophys. J. Suppl. Ser.*, 188(2):384–404, June 2010. doi: 10.1088/0067-0049/

188/2/384.

A. P. Schoenmakers et al. *Mon. Not. R. Astron. Soc.*, 315:371–380, June 2000. doi: 10.1046/j.1365-8711.2000.03430.x.

B. Sebastian et al. *Mon. Not. R. Astron. Soc.*, 530(4):4902–4919, June 2024. doi: 10.1093/mnras/stae546.

S. Sethi, A. Kuźmicz, D. Hunik, and M. Jamrozy. *A&A*, 699(L4):L4.1 – L4.7, July 2025. doi: 10.1051/0004-6361/202554987.

S. S. Shabala et al. *Mon. Not. R. Astron. Soc.*, 496(2):1706–1717, Aug. 2020. doi: 10.1093/mnras/staa1172.

S. S. Shabala et al. *Publ. Astron. Soc. Aust.*, 41:e024, Jan. 2024. doi: 10.1017/pasa.2024.11.

N. I. Shakura and R. A. Sunyaev. *A&A*, 24:337 – 355, June 1973.

T. W. Shimwell et al. *Astron. Astrophys.*, 707:A198, Mar. 2026. doi: 10.1051/0004-6361/202557749.

V. Singh, S. Dutta, Y. Wadadekar, and C. H. Ishwara-Chandra. *Galaxies*, 9(4):121, Dec. 2021. doi: 10.3390/galaxies9040121.

O. B. Slee et al. *Astron. J.*, 122(3):1172–1193, Sept. 2001. doi: 10.1086/322105.

V. Smolčić et al. *Astron. Astrophys.*, 602:A1, June 2017. doi: 10.1051/0004-6361/201628704.

M. Stimpson, M. J. Hardcastle, and M. G. H. Krause. *Mon. Not. R. Astron. Soc.*, 539(2):1668–1691, May 2025. doi: 10.1093/mnras/staf610.

M. R. Swain, A. H. Bridle, and S. A. Baum. *Astrophys. J. Lett.*, 507(1):L29–L33, Nov. 1998. doi: 10.1086/311663.

F. Sweijen et al. *Mon. Not. R. Astron. Soc.*, 540(1):416–432, June 2025. doi: 10.1093/mnras/staf630.

P. C. Tribble. *Mon. Not. R. Astron. Soc.*, 250:726, June 1991. doi: 10.1093/mnras/250.4.726.

P. C. Tribble. *Mon. Not. R. Astron. Soc.*, 261:57, 1993.

R. J. Turner and S. S. Shabala. *Astrophys. J.*, 806(1):59, June 2015. doi: 10.1088/0004-637X/806/1/59.

R. J. Turner and S. S. Shabala. *Mon. Not. R. Astron. Soc.*, 493(4):5181–5194, Apr. 2020a. doi: 10.1093/mnras/staa702.

R. J. Turner and S. S. Shabala. *Mon. Not. R. Astron. Soc.*, 493(4):5181–5194, Apr. 2020b. doi: 10.1093/mnras/staa702.

R. J. Turner and S. S. Shabala. *Galaxies*, 11(4):87, July 2023. doi: 10.3390/galaxies11040087.

R. J. Turner, J. G. Rogers, S. S. Shabala, and M. G. H. Krause. *Mon. Not. R. Astron. Soc.*, 473(3):4179–4196, Jan. 2018. doi: 10.1093/mnras/stx2591.

F. Ubertosi et al. *Astron. Astrophys.*, 688:A86: 1–19, Aug. 2024. doi: 10.1051/0004-6361/202349011.

E. Vardoulaki et al. *Astron. Astrophys.*, 627:A142, July 2019. doi: 10.1051/0004-6361/201832982.

E. Vardoulaki et al. *Astron. Astrophys.*, 648:A102, Apr. 2021. doi: 10.1051/0004-6361/202039488.

J. F. C. Wardle and S. E. Aaron. *Mon. Not. R. Astron. Soc.*, 286(2):425–435, Apr. 1997. doi: 10.1093/mnras/286.2.425.

P. M. Yates-Jones et al. *Publ. Astron. Soc. Aust.*, 40:e014, Apr. 2023. doi: 10.1017/pasa.2023.10.

S. A. Young et al. *Publ. Astron. Soc. Aust.*, 42:e100, July 2025. doi: 10.1017/pasa.2025.10068.

Z. S. Yuan, X. Y. Gao, Z. L. Wen, and J. L. Han. *RAA*, 24(4):4.1 – 4.7, Apr. 2024.